

Urban Air Mobility Guidance with Panel Method: Experimental Evaluation under Wind Disturbances

Zeynep Bilgin*

Technical University of Munich, Garching, 85748, Germany

Murat Bronz†

ENAC, École Nationale de l'Aviation Civile, Université de Toulouse, Toulouse, 31400, France

Ilkay Yavrucuk‡

Technical University of Munich, Garching, 85748, Germany

In this paper, a nature-inspired guidance algorithm based on panel method is proposed. Panel method is a numerical tool borrowed from the aerodynamics domain to calculate the potential field of a fluid flow around arbitrarily shaped objects. The proposed algorithm has little computational load and generates guidance vectors in real-time that can guide multiple vehicles through smooth and collision-free paths. Panel method-based guidance is a promising candidate for air mobility applications in urban environments where multiple aerial vehicles are expected to operate simultaneously without colliding with architectural structures and other vehicles in the airspace. In this study, the effectiveness and feasibility of the proposed guidance method is evaluated through a test campaign conducted in Toulouse, France, using multiple quad-rotors in a scaled urban environment. Furthermore, the robustness of the guidance method under wind disturbances is tested in both indoor and outdoor experiments. Experimental results suggest that panel method based guidance algorithm is an effective and robust tool for real-time, collision-free guidance of multiple aerial vehicles in complex urban environments.

Supplementary video: <https://youtu.be/tYDMfPYLinQ>

I. Nomenclature

K = Coefficient matrix

x, y , or d = Distance

A version of this work was presented in AIAA Aviation Forum, 27 June - 1 July 2022, Chicago, Illinois, USA with paper ID AIAA 2022-3509.
*PhD Candidate, Institute of Helicopter Technology and VTOL, TUM School of Engineering and Design, zeynep.bilgin@tum.de, AIAA Student Member.

†Assistant Professor, ENAC-Lab, Dynamic Systems, murat.bronz@enac.fr, AIAA Member.

‡Professor, Institute of Helicopter Technology and VTOL, TUM School of Engineering and Design, ilkay.yavrucuk@tum.de, AIAA Member.

q	=	Flow velocity induced by a vortex
u and v	=	Flow velocity components
N	=	Number of aerial vehicles
β	=	Panel orientation angle
s	=	Panel length
Γ or γ	=	Vortex strength
I	=	Inertia matrix
Ω	=	Angular rates
f and g	=	Functions
G	=	Control effectiveness matrix
ν	=	Virtual control
Subscript	=	Meaning
∞	=	Free stream
i and j	=	Panel number
$sink$	=	Sink element
$source$	=	Source element

II. Introduction

ADVANCES in automation and electric storage encouraged growth in urban aviation industry. Utilizing aerial vehicles for the transport of people and goods over short distances in urban areas could make a contribution to mobility in the future. Aerial vehicles with different designs, sizes, maneuverability, automation levels and communication capabilities will be competing for same limited urban air space previously unregulated. This new demand urges industry, cities and governments come up with new air traffic management scheme [1]. Having fully autonomous vehicles that can generate collision free paths not only increases the capacity of the urban airspace but also reduces the urban air traffic management efforts [2]. Therefore, path planning and guidance in urban environments is an important issue to be addressed.

Recent studies addressed path planning problem in urban environment [3–6]. However, as urban air mobility concept is relatively new, path planning applications in this area is limited. On the other hand, path planning for unmanned aerial vehicles (UAV) is well studied in literature. Therefore, to have a better insight on path planning schemes literature review is conducted irrespective of operation environment. Classical approaches to path planning for autonomous vehicles can be divided into three sub-categories: reactive methods, optimization problem based methods and potential field based methods. Reactive methods are suitable for dynamic environments and search safe avoidance maneuvers taking

into account the velocity and/or acceleration of the obstacles [7–13]. Second approach is formulating the problem as a large optimization problem with constraints. Constraints may include dynamics of the vehicle and air traffic regulations. Different cost functions can be considered to optimize time, distance, energy consumption, number of maneuvers, etc. [14–17]. Third approach is employing artificial potential functions where repulsive functions prevent collisions and attractive functions guide the vehicle to its destination [18]. Potential field approach for path planning is applied in various fields from wheeled ground vehicles to unmanned aerial vehicles [15, 19–23]. Main advantage of this approach is its simplicity and easy implementation. Furthermore, it is possible to further enhance the effectiveness of potential field based methods by combining them with other classical or heuristic approaches [24–27]. The potential field method suffers from two major drawbacks. First one, the vehicle may get trapped in a local minima and secondly, the vehicle cannot reach to its destination if there are obstacles nearby due their repulsive force [28, 29]. Harmonic potential fields, a sub category of potential field based approaches, overcome the local minima limitation and produce constrained and well-behaved robot trajectory in static and dynamic environments [30–35]. One specific harmonic potential field that can be used in path planning is potential field of an irrotational flow of an ideal fluid [23, 36]. The idea to imitate the behavior of gases and fluids has been previously investigated. Models from fluid dynamics have been used in design of feedback control laws for swarms of robots [37]. Similarly, a multi-vehicle flocking and guidance control scheme is proposed by endowing fluid properties to the vehicle swarm [38]. For potential flow based guidance models, analytical solutions can be obtained by combining elementary potentials such as uniform flow, sink and source elements; however, these solutions can only be used to generate a flow field around relatively simple geometries, such as circle and ellipses [39, 40].

In the context of urban air mobility, where obstacles can have complex shapes, classical potential field methods, especially those using circular representations, may become inefficient in cluttered environments. To address this, Collision Cone approach have been proposed in literature [11–13]. Collision Cone methods is a local path planning method that uses geometric representations to avoid obstacles in the immediate surroundings of a mobile robot where collision cones are generated for the vehicle and the obstacle and maneuvers that avoid these cones are selected. It is especially well-suited for dynamic environments with arbitrarily shaped obstacles [12]. Alternatively, a global path planning approach using harmonic potential fields can be extended to arbitrarily shaped obstacles by utilizing a numerical method, namely panel method borrowed from aerodynamics domain [40, 41]. Panel method was previously used for motion planning for ground robots [31, 42, 43].

Air mobility in urban environments indicate high number of operations at low altitudes. That means aerial vehicles operating in urban environments are expected to safely avoid collision with both complex shaped architectural structures, other vehicles operating in the same limited airspace as well as any dynamic obstacles that can pop-up. Guidance problem in such environments become mathematically large in size and computationally expensive. Therefore, methods that guarantee obstacle avoidance and collision avoidance while providing fast solutions to real-time guidance for

multiple aerial vehicles in urban airspace are valuable [44]. In this paper panel method based guidance algorithm is proposed to be used for real-time path planning for air mobility in urban environments. Panel method has little computation load; thus, it is suitable for real-time applications [44]. Moreover, the proposed method utilizes harmonic potential fields which inherently guarantee collision avoidance and convergence to goal position without getting trapped in a local-minima [30, 31]. These properties make panel method based guidance algorithm a promising candidate for air mobility applications in urban environments.

Experimental evaluation of guidance methods is essential to validate the effectiveness and robustness of proposed algorithms. In this study, performance of the proposed panel method based guidance algorithm is evaluated through hardware experiments conducted in Toulouse, France. Hardware experiments are conducted for both indoor and outdoor scenarios using quad-rotors. Indoor flights took place in The Toulouse Occitanie Drone Flight Arena located in France. The flight area that is equipped with high-precision localisation and measuring instruments is one of the most hi-tech instrument equipped indoor flight zones in Europe [45]. Scaled buildings with various shapes are produced and placed in the 8x8 flight arena to model a scaled urban environment. Furthermore, indoor tests are conducted under wind disturbance to assess the robustness of the proposed method. To better evaluate performance under sensor uncertainties and wind disturbances outdoor tests are conducted. Outdoor experiments are held in a local RC airfield runway located in Muret, France. Panel method based guidance algorithm can easily be scaled to larger problems. Thanks to this property, in outdoor experiments, quad-rotors were able to fly in a much larger area compared to indoor tests.

Main contributions of this study are as follows:

- Utilizing panel method, a numerical tool for calculating potential field of a fluid flow around obstacles, as a real-time guidance method for multiple aerial vehicles in an urban environment. Additional flow elements are included in conventional panel method equations to satisfy the needs of guidance problem. To represent goal positions point sink elements are used and to prevent collision with other vehicles a point source element is assigned to each vehicle.
- Introduction of *safety source element*: Although trajectories tangent to obstacle boundaries are valid solutions for fluid dynamics, it is not a feasible solution for path planning of aerial vehicles. To generate safer paths that are not tangent to obstacles an additional source element that travels with the vehicle itself is introduced. This novel *safety source element* can generate trajectories as far away from obstacles as desired while still guaranteeing convergence to goal position.
- Introduction of a correction term during velocity calculation step in order to improve disturbance rejection performance of panel method based guidance algorithm.
- Experimental evaluation of the panel method based guidance algorithm. Hardware experiments for both indoor and outdoor scenarios are conducted to assess the performance of the proposed method in real-time scenarios in a

scaled urban environment.

- Robustness performance assessment of panel method based guidance under wind disturbances and sensor errors.

III. Panel Method Based Guidance Methodology

A. Panel Method Preliminaries

Panel methods are well-known numerical tools used in aerodynamics domain for solving Laplace's equation for irrotational flow of an ideal fluid around arbitrarily shaped objects. Since Laplace's equation is linear, potential flow elements that satisfy the Laplace's equation can be superposed. Panel method relies on this property to divide surface of an object into discrete potential flow elements called 'panels' (hence, the name 'panel' method.) and superposing each element to calculate the flow velocity field around the object [40, 41].

Following [40, 46], let \mathcal{D} be a region in \mathbb{R}^2 containing an ideal fluid and $\mathbf{P} = (x, y)^T$ be an arbitrary point in \mathcal{D} . Let $\mathbf{V} = (u, v)^T$ denote the instantaneous velocity of the fluid at any point in \mathcal{D} . By Biot-Savart Law, velocity induced by a point vortex element placed at a point $\mathbf{P}_j = (x_j, y_j)^T$ on any point $\mathbf{P} = (x, y)^T \in \mathcal{D}$ can be calculated in terms of unknown vorticity strength γ_j as shown in Equation 1, [40].

$$\begin{bmatrix} u \\ v \end{bmatrix} = \frac{\gamma_j}{2\pi r_{pj}^2} \begin{bmatrix} 0 & 1 \\ -1 & 0 \end{bmatrix} \begin{bmatrix} x_j - x \\ y_j - y \end{bmatrix} \quad (1)$$

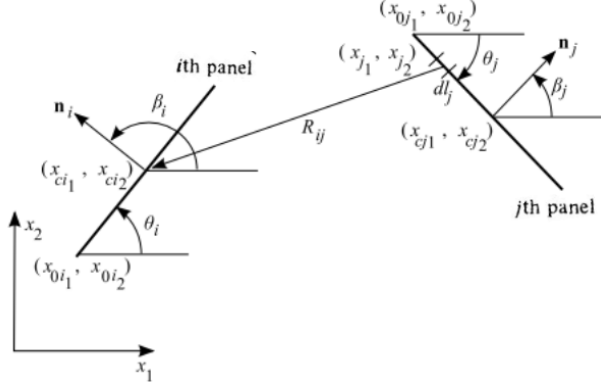
where $(x_j, y_j)^T$ denotes the position of the point vortex and $r_{pj} = \sqrt{(x - x_j)^2 + (y - y_j)^2}$ is the Euclidean distance between point vortex element and the point $\mathbf{P} = (x, y)^T$.

Velocity calculation formula given in Equation 1 can be applied to calculation of velocity induced by panels on an obstacle surface. In Figure 1b an arbitrarily shaped object with surface divided into a number of panels is presented. In Figure 1a sign convention for panel orientation angles and surface normals are given.

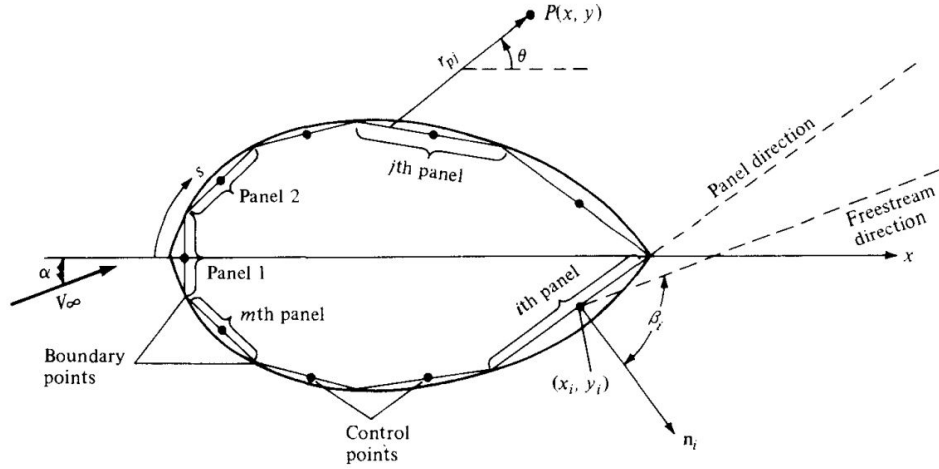
For this study, prescribed flow elements on panels are selected as point vortices and placed on collocation points, $\mathbf{P}_{cj} = (x_{cj}, y_{cj})^T$ as shown in Figure 1a. Velocity induced by a vortex element placed on j th panel at $\mathbf{P}_{cj} = (x_{cj}, y_{cj})^T$ on i th panel at $\mathbf{P}_{ci} = (x_{ci}, y_{ci})^T$ can be calculated as $\mathbf{V}_{ij} = (u, v)_{ij}$ using the relation given in Equation 1, [40].

In order to find the unknown vorticity on obstacle surface, a Dirichlet boundary condition has to be enforced; the normal velocity induced at each panel on the object surface has to be zero. That is, flow cannot go into or out of the object surface. After applying the boundary condition for each panel, the unknown vorticity problem can be expressed as a system of linear equations given in Equation 2, [40].

$$K_{ij}\gamma_j = RHS_i \quad (2)$$



(a) Sign convention for panel orientation angles and surface normals [33]



(b) Panel distribution over the surface of a body of arbitrary shape [41].

Fig. 1 Panel distribution on an arbitrarily shaped obstacle and sign conventions of panel angles.

$$K_{ij}\gamma_j = (u, v)_{ij} \cdot \vec{n}_i \quad (3)$$

Here, K is a coefficient matrix and γ_j is the unknown vortex strength on panel j . $K_{ij}\gamma_j$ is the normal component of the velocity induced by j th panel on i th panel as given in Equation 3. Note that, the coefficient matrix K is a known matrix and composed of geometrical properties of panels such as their respective orientations and positions.

The vector RHS consists of normal component of velocity induced by other known potential flow elements in \mathcal{D} . In aerodynamics, RHS usually contains only the normal component of free stream velocity $V_\infty = (u_\infty, v_\infty) \cdot \vec{n}_i$ as in Equation 4, [40, 41]. Here, the angle β_i is the orientation of panel surface normal as shown in Figure 1a and free stream velocity V_∞ is shown in Figure 1b.

$$RHS_i = -u_\infty \cos \beta_i - v_\infty \sin \beta_i \quad (4)$$

After solving Equation 2 for unknown vortex strengths γ_j , flow velocity at any point $\mathbf{P} = (x, y)^T$ in \mathcal{D} can be calculated using Equation 1 for every panel on obstacle surface and superposing the resultant velocities [40]. Panel methods are

well studied in fluid mechanics and aerodynamics domain. Reader may refer to [40, 41] for detailed derivation of panel method.

B. Panel Method Application in Guidance Problem

The solution of any given problem can be numerically calculated using panel methods as long as the velocity potential satisfies the Laplace's equation. Therefore, a guidance potential field around arbitrarily shaped obstacles can be defined using panel method.

In order to fit the needs of the guidance problem, *RHS* vector in Equation 2 has to be further modified.

1. Defining a Goal Position

First, a point sink element is introduced to represent a goal position for the vehicle. Let $\mathbf{P} = (x, y)^T$ be an arbitrary point in \mathcal{D} and $\mathbf{P}_g = (x_g, y_g)^T \in \mathcal{D}$ be the known goal position of a vehicle where a point sink element is placed with known strength, σ_g . Then, the velocity induced at point $\mathbf{P} = (x, y)^T$ by the sink element at $\mathbf{P}_g = (x_g, y_g)^T$ can be calculated using the formula given in Equation 5

$$\begin{bmatrix} u_{sink} \\ v_{sink} \end{bmatrix} = \frac{-\sigma_g}{2\pi r_g^2} \begin{bmatrix} x - x_g \\ y - y_g \end{bmatrix} \quad (5)$$

Then, velocity induced by the point sink element (u_{sink} and v_{sink}) can be included to *RHS* vector as shown in Equation 6

$$RHS_i = -u_\infty \cos \beta_i - v_\infty \sin \beta_i - u_{sink} \cos \beta_i - v_{sink} \sin \beta_i \quad (6)$$

2. Guaranteeing Collision Avoidance

The guidance vector field has built in obstacle avoidance property due to the boundary condition of zero normal velocity at panel collocation points on obstacle surfaces imposed on panel method equations, given that sufficient number of panels are defined on the obstacle boundary. However, avoiding collisions between vehicles is just as important in a guidance problem when multiple agents are involved. To prevent collisions between aerial vehicles, each aerial vehicle is modeled as a point source element. Let $\mathbf{P}_n = (x_n, y_n)^T$ be the position of the n^{th} vehicle in a fleet with N vehicles. Then, the velocity induced by a point source element at $\mathbf{P}_n = (x_n, y_n)^T$ with known strength σ_n on any point $\mathbf{P} = (x, y)^T \in \mathcal{D}$ can be calculated using the formula given in Equation 7

$$\begin{bmatrix} u_{source}^n \\ v_{source}^n \end{bmatrix} = \frac{-\sigma_n}{2\pi r_n^2} \begin{bmatrix} x - x_n \\ y - y_n \end{bmatrix} \quad (7)$$

The velocity induced by the source elements on each vehicle can be added and included in RHS vector as in Equation 8.

$$RHS_i = -u_\infty \cos \beta_i - v_\infty \sin \beta_i - \sum_{n=1}^N u_{source}^n \cos \beta_i - \sum_{n=1}^N v_{source}^n \sin \beta_i - u_{sink} \cos \beta_i - v_{sink} \sin \beta_i \quad (8)$$

3. Defining a Safety Perimeter Around Obstacles

The zero normal velocity boundary condition on panel method equations indicate that, streamlines(trjectories) tangent to obstacle boundaries are valid solutions for panel method. However, for guidance purposes where vehicles have finite volume; trajectories tangent to obstacle boundary are not valid. One possible solution is to expand the obstacle boundary with the amount equal to or greater than vehicle size. To increase the safety perimeter around the obstacles *safety source element* introduced in [47] is included in RHS vector in Equation 9.

$$RHS_i = -u_\infty \cos \beta_i - v_\infty \sin \beta_i - \sum_{n=1}^{N_{eVTOL}} u_{source}^n \cos \beta_i - \sum_{n=1}^{N_{eVTOL}} v_{source}^n \sin \beta_i \\ - u_{sink} \cos \beta_i - v_{sink} \sin \beta_i - u_{safety} \cos \beta_i - v_{safety} \sin \beta_i \quad (9)$$

The *safety source element* is a point source element that travels with the vehicle itself. This additional source element causes amplified the vortex strengths on the obstacles in the vicinity of the vehicle. The *Safety source element* is only used in unknown vortex strength calculations and not included in velocity vector calculations so that resultant amplified vortex elements prevent the tangent solution. One of the main advantages of using the *safety source element* is that

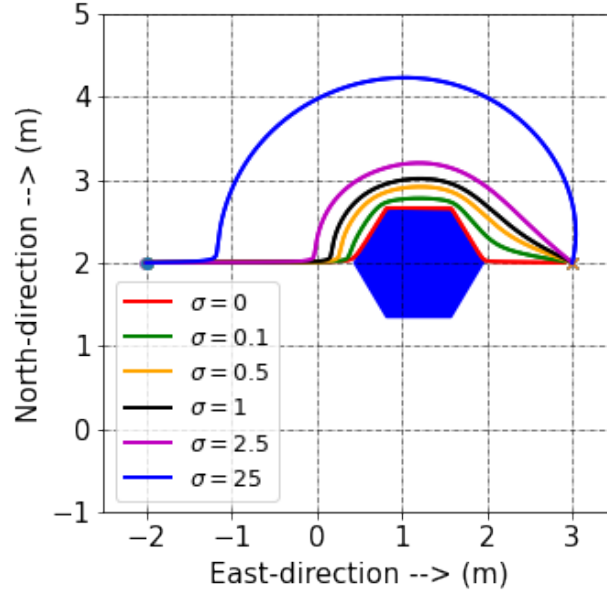


Fig. 2 Paths generated with safety source elements with strengths ranging from $\sigma = 0$ to $\sigma = 25$ [47].

it gives the designer flexibility to control the safety perimeter around the obstacles. Effect of *safety source element*

is demonstrated in Fig. 2. In this figure resultant paths generated with *safety source element* with strengths ranging from $\sigma = 0$ to $\sigma = 25$ are plotted. As the strength of the *safety source element* increases, a path further away from the obstacle is generated without sacrificing the convergence to the goal position. A similar effect could have been achieved by adjusting the expansion radius of obstacles. However, when obstacle shapes change, the coefficient matrix given in Equation 2 has to be recalculated and inverted again; this would bring a large computational burden. Instead, since *safety source element* only appears in calculations as an additional source element, it has negligible computational burden and can be adjusted even online. Furthermore, since it is a source element attached to the vehicle, each vehicle can have a different *safety source element*; hence, vehicles can have different safety perimeters around obstacles depending on their performance specifications. For example, vehicles with high maneuverability can be assigned smaller *safety source element* and less agile vehicles can be assigned larger *safety source element*. This would enable operating multiple vehicles with varying capabilities in the same framework without sacrificing safety or performance. This capability would be especially useful in urban air mobility applications where vehicles with different capabilities are expected to operate in the same airspace.

4. Calculating the Flow Velocity

After finding the unknown vortex strengths by solving the Equation 2, flow velocity $\mathbf{V} = (u, v)^T$ at any point $\mathbf{P} = (x, y)^T \in \mathcal{D}$ can be calculated using the relations given in Equation 10 and Equation 11.

$$u = \frac{-\sigma_g}{2\pi} \frac{x - x_g}{r_g^2} + \sum_{n=1}^N \frac{\sigma_n}{2\pi} \frac{x - x_n}{r_n^2} + \sum_{s=1}^S \sum_{k=1}^K \frac{\gamma_{sk}}{2\pi} \frac{x - x_{sk}}{r_{sk}^2} + u_\infty \quad (10)$$

$$v = \frac{-\sigma_g}{2\pi} \frac{y - y_g}{r_g^2} + \sum_{n=1}^N \frac{\sigma_n}{2\pi} \frac{y - y_n}{r_n^2} + \sum_{s=1}^S \sum_{k=1}^K \frac{-\gamma_{sk}}{2\pi} \frac{y - y_{sk}}{r_{sk}^2} + v_\infty \quad (11)$$

Here, u_∞ and v_∞ are components of the free stream velocity. The goal position is denoted by $\mathbf{P}_g = (x_g, y_g)^T$ and sink strength associated with this goal position is σ_g . N is the total number of aerial vehicles in the fleet and source with strength σ_n is assigned to each vehicle to prevent collisions. Position of vehicles are denoted as $\mathbf{P}_n = (x_n, y_n)^T$. S and K are number of obstacles and number of panels on obstacle surfaces respectively. Position of a vortex element on a given obstacle and panel is denoted as (x_{sk}, y_{sk}) and associated vortex strength is γ_{sk} .

C. Panel Method and Automatic Flight Controller Integration for Guidance

Block diagram for panel method based guidance is presented in Figure 3. Panel method requires vehicle positions, goal position and obstacle vertices as input. First, the obstacle boundary is divided into small line segments and vortex elements with unknown strength is assigned to each line segment. Point source and point sink elements with known

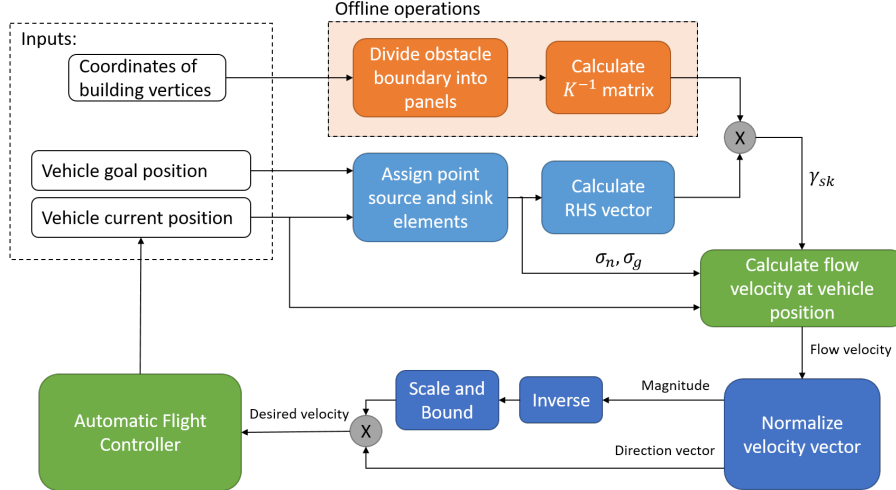


Fig. 3 Block diagram for panel method based guidance.

strength are assigned to vehicles and goal positions respectively. Next, equation 2 has to be solved for unknown vortex strengths. Coefficient matrix K in Equation 2 only depends on obstacle shape and can be calculated and inverted offline to reduce computational load. After vortex strengths are found, flow velocity at current vehicle position can be calculated using Equation 10 and Equation 11. At this step, positions of other vehicles are also required for collision avoidance calculations. As every vehicle has to account for all other vehicles in the arena, computational load of this algorithm increases quadratically with increasing number of vehicles.

Flow velocity is greater in narrow passages and near goal position; however, the opposite velocity regime is safer and more desirable for vehicles. In order to achieve a more desirable velocity profile, first, Euclidean norm of flow velocity vector is calculated as given in Equation 12.

$$\|\mathbf{V}\| = \sqrt{u^2 + v^2} \quad (12)$$

Here, $\mathbf{V} = (u, v)^T$ denote the non-zero instantaneous velocity of the fluid at any point. Normalized flow velocity is then $\bar{\mathbf{V}} = \mathbf{V}/\|\mathbf{V}\|$. Finally, the desired velocity to be fed into the automatic flight controller can be calculated as in Equation 13. Here, c is a scaling constant that depends on arena size and maximum allowable speed for vehicles.

$$V_{des} = c \|\mathbf{V}\|^{-1} \bar{\mathbf{V}} \quad (13)$$

The controller used in this study is based on the work [48]. Brief summary of the control method is presented here. The method relies on the control of the angular accelerations in an *incremental* way. First, consider the angular acceleration of the vehicle. Neglecting the gyroscopic moments, the angular acceleration of the vehicle becomes a

function of the angular rate, airspeed, and the input vector \mathbf{u} as in Equation 14, [48].

$$\mathbf{I}\dot{\boldsymbol{\Omega}} = \mathbf{f}(\boldsymbol{\Omega}, \mathbf{v}) + \mathbf{g}(\mathbf{u}) \quad (14)$$

where \mathbf{I} is the moment of inertia matrix, $\boldsymbol{\Omega}$ is the angular rate vector and \mathbf{v} is the airspeed vector. First order Taylor series expansion of Equation 14 is given in Equation 15

$$\mathbf{I}\dot{\boldsymbol{\Omega}} = \mathbf{I}\dot{\boldsymbol{\Omega}}_0 + \frac{\partial}{\partial \boldsymbol{\Omega}}\mathbf{f}(\boldsymbol{\Omega}, \mathbf{v}_0)|_{\boldsymbol{\Omega}=\boldsymbol{\Omega}_0}(\boldsymbol{\Omega} - \boldsymbol{\Omega}_0) + \frac{\partial}{\partial \mathbf{v}}\mathbf{f}(\boldsymbol{\Omega}_0, \mathbf{v})|_{\mathbf{v}=\mathbf{v}_0}(\mathbf{v} - \mathbf{v}_0) + \frac{\partial}{\partial \mathbf{u}}\mathbf{g}(\mathbf{u})|_{\mathbf{u}=\mathbf{u}_0}(\mathbf{u} - \mathbf{u}_0) \quad (15)$$

Here, the angular acceleration depends on the current angular acceleration, the partial derivatives of the functions \mathbf{f} and \mathbf{g} and the change in state and inputs. Considering only a small time interval, but long enough for the actuators to adopt their new values, the change in $\boldsymbol{\Omega}$ and \mathbf{v} and their respective derivatives can be neglected. Dividing by \mathbf{I} and assuming that the partial derivative of \mathbf{g} with respect to \mathbf{u} is a static matrix for some part of the flight envelope, angular acceleration can be approximated as given in Equation 16, [48].

$$\dot{\boldsymbol{\Omega}} = \dot{\boldsymbol{\Omega}}_0 + \mathbf{G}(\mathbf{u} - \mathbf{u}_0) \quad (16)$$

where \mathbf{G} is the control effectiveness matrix, which contains the effectiveness of each actuator on each axis. Its values are determined with a least squares fit with changes in input and angular acceleration obtained from flight data. The control law can be obtained by inverting Equation 16.

$$\mathbf{u} = \mathbf{u}_0 + \mathbf{G}^{-1}(\mathbf{v} - \dot{\boldsymbol{\Omega}}_0) \quad (17)$$

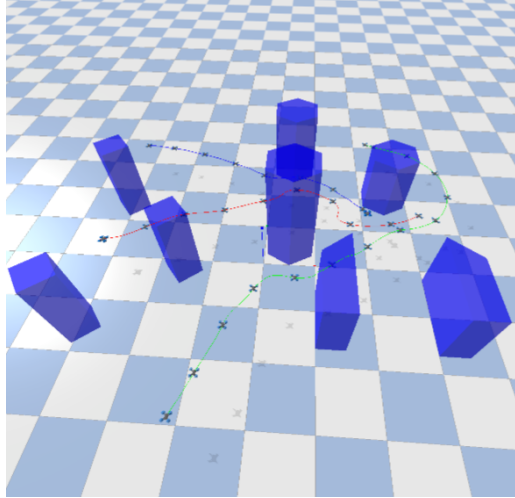
Here, the desired angular acceleration, $\dot{\boldsymbol{\Omega}}$, has become the virtual control \mathbf{v} . A PD controller that will provide the virtual control; that is, the desired angular acceleration can be designed to control the attitude. Detailed explanation on controller design can be found in [48].

IV. Experimental Setup

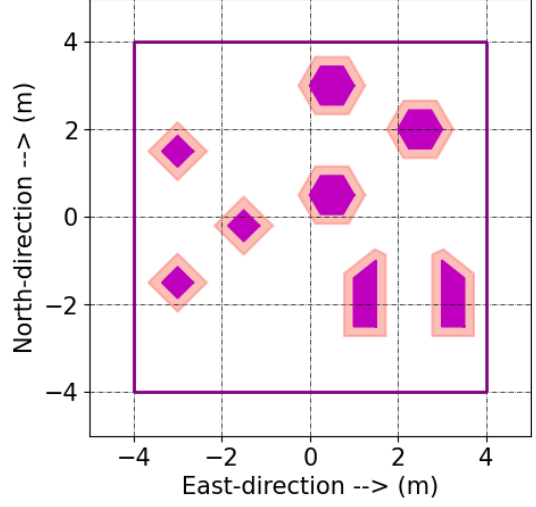
One of the main contributions of this study is the experimental demonstration of the proposed method and verification of its robustness to unknown wind disturbance. For both indoor and outdoor experiments, ENAC's existing infrastructure for autonomous systems is utilized. This section briefly explains the simulation environment used in development, the autopilot system, indoor and outdoor flight setup, and wind generation method.

A. Simulation Environment

A simulation environment, shown in Fig. 4a, based on pyBullet is used with the architecture suggested in [49]. Simulation environment includes vehicle dynamics as well as a simplified rotor dynamics model. Rotor force and torque is modelled proportional to propeller rotational speed as $F_r = k_f \omega^2$, and $Q_r = k_q \omega^2$ respectively, where ω is the propeller rotation rate [49]. High incidence angle conditions are not taken into account.



(a) Simulation environment based on pyBullet[49].



(b) 2-D cross-section of the arena.

Fig. 4 Simulation environment and the arena used in simulations and hardware tests.

Arena plotted in Fig. 4b is used for both simulations and hardware experiments. Geometric shapes in Fig. 4b represent the cross-sections of various buildings in an urban environment. Although panel method can handle any arbitrarily shaped obstacle; square, hexagon and trapezoid obstacles are selected for ease of manufacture in hardware experiments. As a safety precaution, obstacle boundaries are inflated by an amount equal to vehicle radius. In Fig. 4b solid magenta shapes are real obstacles and shaded areas are obstacle boundaries obtained after inflation. In panel method calculations, these inflated obstacle boundaries are considered. Horizontal and vertical lines indicate indoor arena limits and x-axis and y-axis are both in meters.

B. Experiment Facilities

1. Indoor Flight Facility

Indoor experiments are conducted in The Toulouse Occitanie Drone Flight Arena located in Toulouse, France as shown in Fig. 5a. Obstacles with various shapes and heights are inserted into the $8m \times 8m \times 8m$ flight area to model a scaled urban environment. Test environment is equipped with 16-camera Optitrack system is used to track the motion of the quadrotors with sub-millimetre resolution in real time—a feature that is replaced by considerably less accurate GPS when flying outdoors.

The quadrotor used in indoor scenarios is called Explorer 1 (shown in Fig. 5b). Including the battery, its mass is 400 g

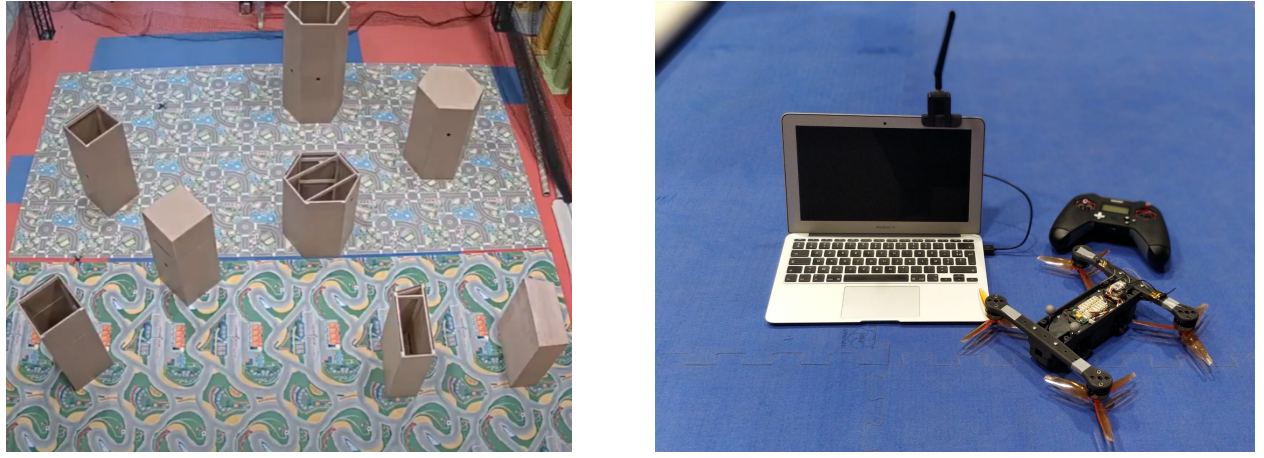


Fig. 5 Indoor flight facility.

and its maximum thrust is 40 N. A 3-cell battery operates at 11.1 V and contains 2,700 mAh, which provides roughly 14 minutes of flight time. Detailed specifications are presented in Table 1.

In the indoor setup, vehicle position and attitude is sensed by the optitrack system and fed to the control computer. Control computer calculates desired velocities and sends this information together with vehicle's own position via wireless communication. Communication scheme for indoor test environment is sketched in Figure 6.

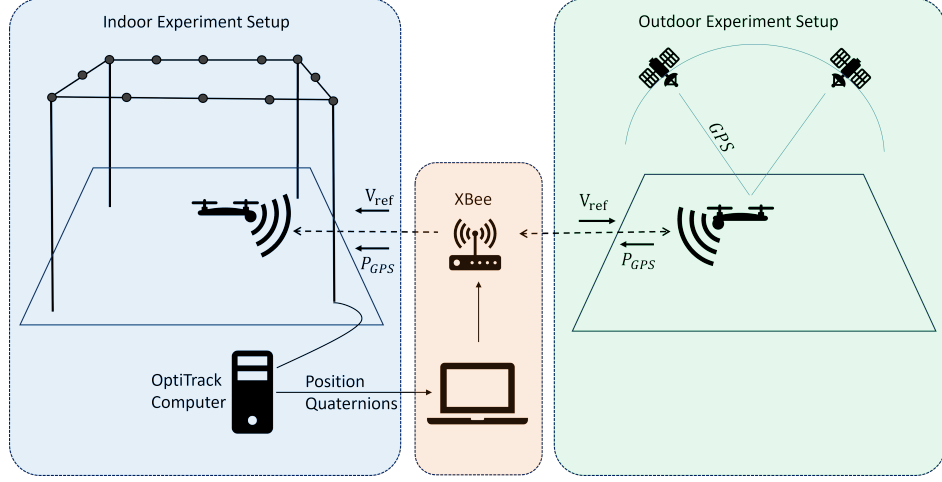


Fig. 6 Communication Scheme for Indoor and Outdoor Experiment Setup.

2. Outdoor Flight Facility

Outdoor runway experiments are conducted in a local RC airfield runway located in Muret, France, that is 124 m × 12.5 m in size, as shown in Fig. 7a. ENAC has privileged access to this airfield, and can do tests in a volume of 500 m

Specification	Units	Paparazzi Quadrotor	
		Indoor	Outdoor
Mass	[g]	400.	440.
Maximum Flight Speed	[m/s]	4.	14.
Flight Duration	[min]	14.	12.
Localization		Optitrack	GPS
Autopilot Software		Paparazzi V.6[50]	
Autopilot Hardware		Tawaki V1.1	
Controller		INDI[48]	
Communication		XBee 2.4GHz	
Motors		T-Motor F40 2400Kv	
Propellers		T-Motor F5146	
Battery		11.1V 2.7Ah LiPo	

Table 1 Specifications of the aerial vehicles used in this work, including the effect of additional hardware parts and software limitations.

radius and up to 120 m height (which can be increased to 450 m in certain cases). Quadrotors used for the outdoor flights consist of the same avionics and propulsion system used on the indoor quadrotors, but they are additionally equipped with Ublox-M8 GPS receiver, hence 40g of additional mass, which supplies 5 Hz position information with an accuracy of approximately 1.5 m. Outdoor quadrotors are shown in Fig. 7b alongside with the ground control station (ordinary laptop), safety-pilot transmitters, and an XBee radio-modem that is used for telemetry and down-link communication. Detailed specifications are presented in Table 1.

In the outdoor setup, there is no optitrack system; hence, vehicle position and attitude is sensed by the GPS. Vehicle communicates its position to the control computer via wireless connection. Control computer calculates desired velocities and sends this information to the vehicle. Communication scheme for outdoor test environment is sketched in Figure 6.



(a) Outdoor flight field located in Muret, France.



(b) Ground control station and the outdoor quadrotor.

Fig. 7 Outdoor flight facility and the outdoor quadrotor.

C. Auxilary Experiment Tools

1. WindShape - The Wind Generator

To test the robustness of the algorithm under effects of unknown wind gusts, the wind generator shown in Fig. 8 is used. *WindShape* is a modular wind generator located inside ENAC's indoor flight facility. Spatial wind control is



Fig. 8 WindShape, wind generator located inside ENAC's indoor flight facility.

possible via *wind pixels*, which are individual counter-rotating small electric fans. These fans have very low moment of inertia compared to traditional wind tunnel fans, making them easier to change the rotation rate, hence rapid variation of the wind speed. However during the presented experiments, the spatial wind speed have been kept constant.

2. Paparazzi Autopilot System

Throughout the whole flight tests, we have used the Paparazzi Autopilot system [50]. It is an open-sourced project started back in 2003 and used by several research groups, academics, and hobbyists. Being one of the first open-source autopilot systems in the world, *Paparazzi* covers all three segments: ground, airborne, and the communication link between them. *Paparazzi* has also its complete flight plan language, where the user can define any possible trajectory using existing commands, such as circle, line, hippodrome, figure-eight, survey, etc. Additionally, any function written in C language can be called from the flight plan and executed. This opens up a lot of application possibilities, such as triggering a navigation procedure via a sensor output. Its integrated ground control station permits to control the flight plan execution, to move waypoints, or change any parameters of the aircraft while in flight.

During both indoor and outdoor flights, the position of the vehicles are known (indoor:OptiTrack, outdoor: GPS plus on-board estimation), and therefore the calculated flow-field velocity for each vehicle serves as a reference velocity to follow. This reference is being updated at a frequency of 10Hz during the flights and once the velocity error between the reference and actual velocity is calculated, it is directly used as an input to the guidance control algorithm. Quadrotors use an Incremental Nonlinear Dynamic Inversion (INDI) [48] based guidance outer-loop to calculate the reference attitude and rotation rate, and later a cascaded INDI inner-loop calculates the required motor rpm increments.

V. Results

A. Simulation Results

In this section, three different simulation scenarios are presented to demonstrate path planning ability of panel method based guidance algorithm.

1. Baseline scenario

A scenario for a single vehicle in an urban environment is presented in Fig. 9. Start position of the vehicle is marked with a circle and the goal position is marked with a cross. The resultant path followed by the vehicle is plotted as a red line. The vector field generated by panel method solution is also plotted in the form of streamlines on the map. Each streamline leads to the desired goal point while avoiding obstacles. That is, for each position on the map the velocity vector calculated by panel method based guidance algorithm leads to the goal position with guaranteed obstacle avoidance. This property makes panel method based guidance algorithm robust against disturbances since even if the vehicle deviates from its path due to some disturbance, at its new position a new velocity vector that leads to goal position is calculated.

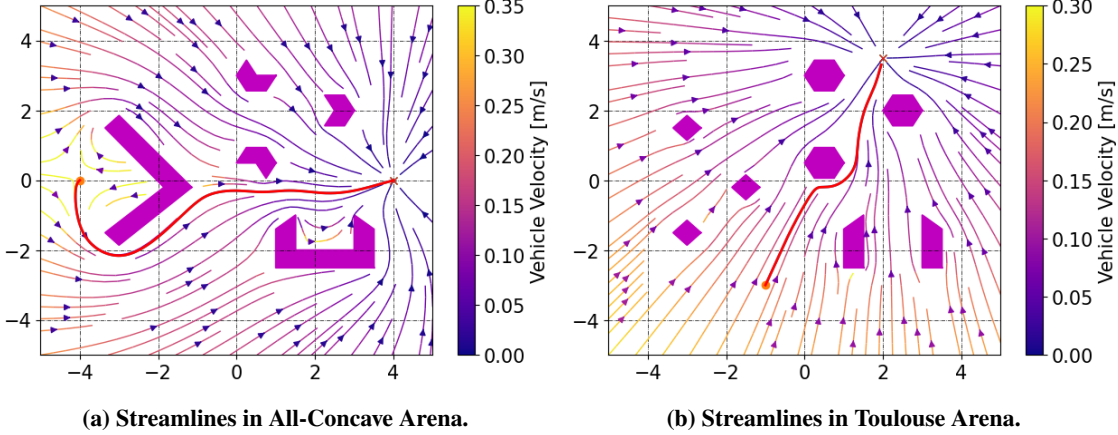


Fig. 9 Streamlines and resultant paths of aerial vehicles in different arenas.

Streamlines and vehicle paths plotted in Fig. 9 are for demonstrating the vector field generated by panel method. In practice, neither streamlines nor the entire vehicle path is calculated. Instead, panel method based guidance algorithm calculates a single velocity vector for the current position of the vehicle. The path plotted in Fig. 9 is the result of following the velocity vectors that are calculated and fed to the vehicle at each position. Panel method based guidance algorithm should not be confused with search algorithms where an optimal path is selected among multiple candidates.

2. Guaranteed global convergence

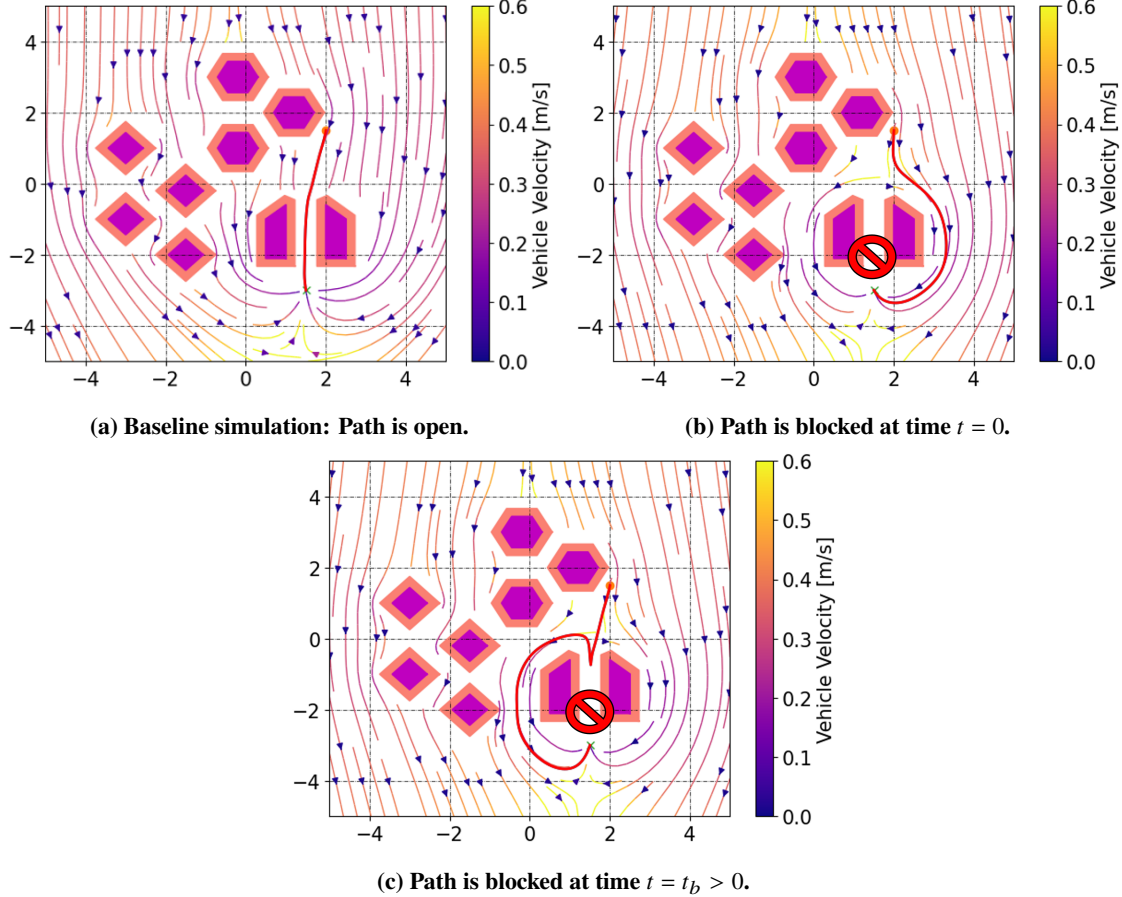


Fig. 10 Streamlines generated by panel method in case of a narrow passage blocked by a virtual obstacle.

The vector field generated by panel method has no local minima and convergence to global minima is guaranteed[30]. In Fig. 10 this property is demonstrated with an example scenario. The baseline simulation is plotted in Fig. 10a where the goal position is set at the end of a narrow passage. Following the streamlines, the vehicle travels through the tunnel between two buildings to arrive at the desired destination. In order to create a possible local minima, a U shaped obstacle is generated by blocking the exit of the tunnel between two trapezoid obstacles as shown in Fig. 10b. Having a priori information about the map; hence, the blockage, panel method generates a path that completely avoids the U shaped obstacle and travels around the buildings to reach desired destination. Finally, in the third case plotted in Fig. 10c, the vehicle has no a priori information about the blocked path. Instead, in an attempt to trap the vehicle inside the U shaped obstacle, the path is blocked after the vehicle enters the tunnel. This time, as soon as the path through the tunnel is blocked, the vehicle turns back and finds an alternate route around buildings to reach its destination.

3. Multiple vehicles

When multiple aerial vehicles are operating at the same time, obstacle avoidance alone is not enough, collision between vehicles should also be prevented. In order to avoid collision between the vehicles, each vehicle is modeled as a point source element that repel other vehicles. Complete knowledge of positions of all aerial vehicles in the fleet is assumed. The source element moves with the vehicle; hence, at every step the vector field needs to be updated with new source position. In Fig. 11 an example scenario where two aerial vehicles intercepting in a narrow passage is plotted. In Fig. 11a no source element is defined for either vehicle and vehicles collide midway. For the second case plotted in Fig. 11b vehicles have equal source strength, $\sigma_1 = \sigma_2 > 0$. This time, vehicles avoid collision while trying to fit into the narrow passage. Source strength is a design parameter and it is possible to assign uneven source strength to vehicles. For the final case, uneven source strength, $\sigma_1 > \sigma_2 > 0$ is assigned to vehicles. Resultant paths are plotted in Fig. 11c. In this configuration, the Blue Vehicle has priority over the Green Vehicle. Hence, the Blue Vehicle takes a shorter path through the narrow passage alone while the Green Vehicle yields and takes a detour around buildings. This type of uneven source assignment could be useful for air traffic management where vehicles have differing capabilities and/or priorities.

In Fig. 12 trajectories of ten aerial vehicles operating at the same time in two different arenas are plotted. The arena plotted in Fig. 12a is Toulouse Arena which is the same arena used in hardware experiments. Second arena plotted in Fig. 12b consist of 15 randomly generated and randomly placed buildings. For both scenarios the vehicles have random start and goal positions. To eliminate trivial scenarios, minimum distance between start and goal positions are set to 1 m. Collision between the vehicles is avoided by source elements assigned to each vehicle. For this scenario, source strengths of the vehicles are also randomized. Notice that, vehicles with greater source strength have higher priority and they inhabit inner regions of the city and travel between buildings whereas vehicles with lower source strength have lower priority and fly longer paths around the city. Panel method based guidance algorithm can successfully solve guidance problem for multiple aerial vehicles simultaneously even in environments dense with obstacles.

B. Indoor Flight Tests

Indoor experiments for this study are conducted in The Toulouse Occitanie Drone Flight Arena located in Toulouse, France (Fig. 5a). The quad-rotor shown in Fig. 5b is used in indoor hardware experiments.

1. Single Vehicle

For the initial hardware experiments, a single vehicle operating in a scaled urban environment is considered. The vehicle is tasked with traveling to 5 different locations consecutively as shown in Fig. 13. The vehicle starts from point E and must circle between positions marked with E-A-B-C-D-E as shown in Fig. 13a. Goal locations and their

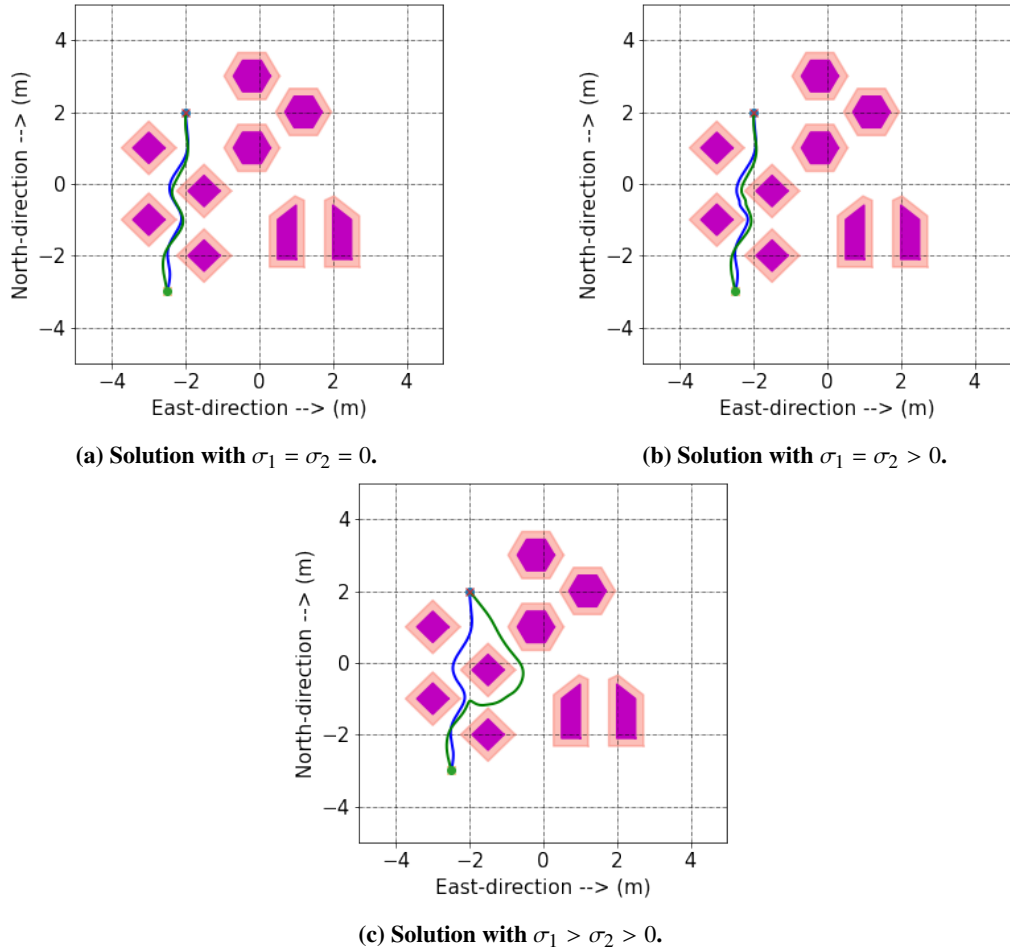


Fig. 11 Simulations with varying source strengths on vehicles through a narrow passage.

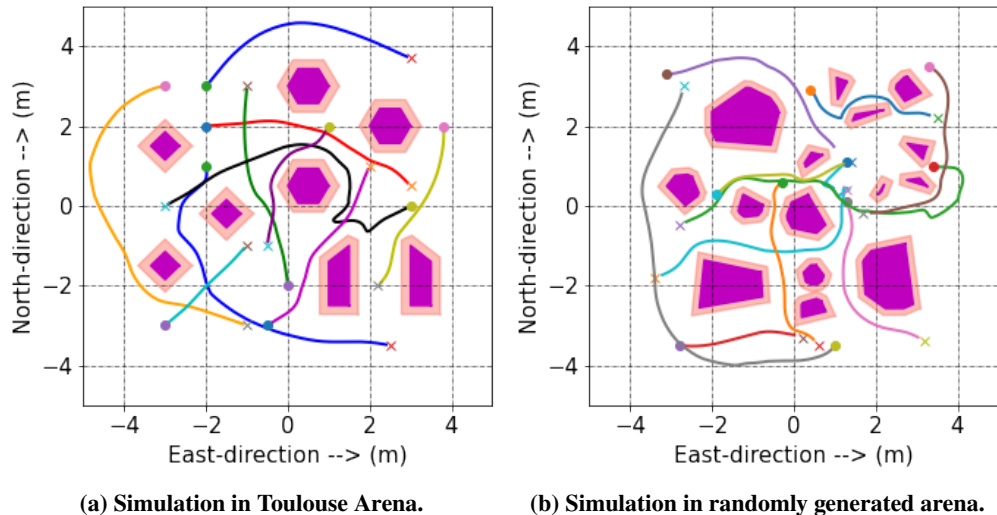


Fig. 12 Randomized simulations with multiple aerial vehicles. All vehicles are assigned a random source strength, $\sigma > 0$.

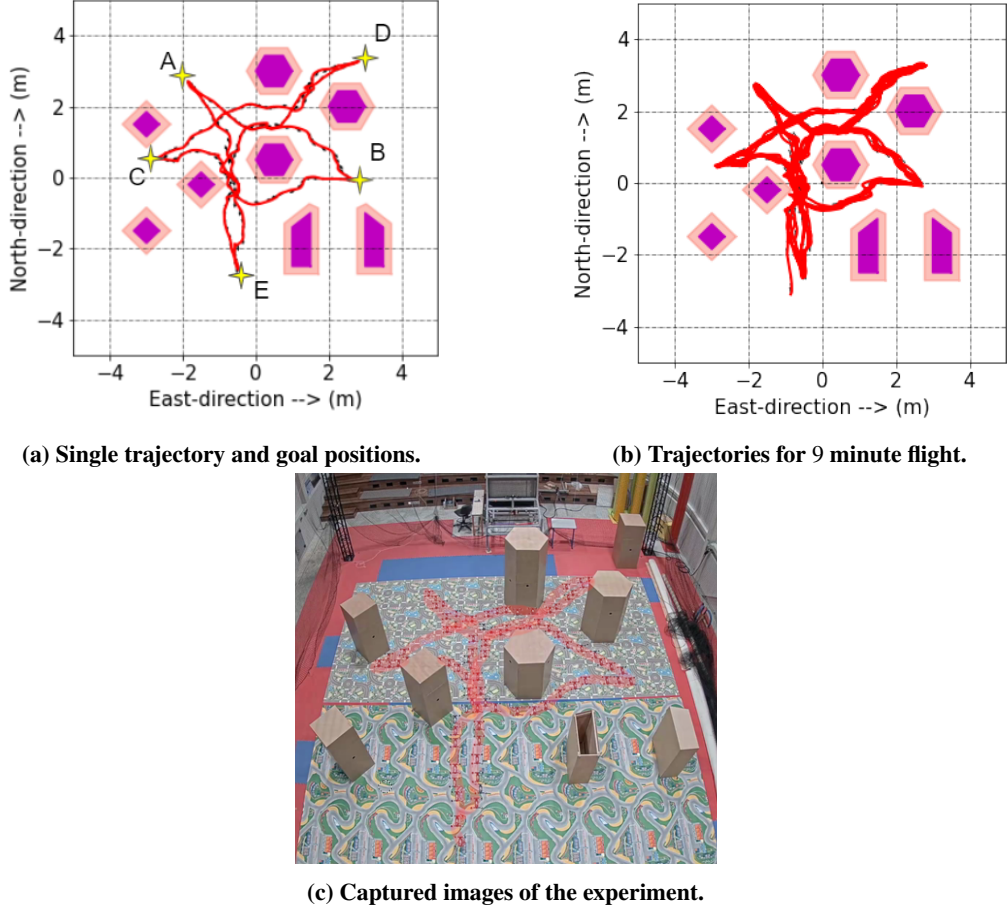


Fig. 13 Experiment 1. The vehicle is tasked with circling between positions marked with E-A-B-C-D-E for 9 minutes while avoiding obstacles.

order is selected such that the vehicle is forced into narrow corridors between buildings to better demonstrate the obstacle avoidance capability of panel method based guidance algorithm. In Fig. 13b, trajectory generated by the vehicle after 9 minute flight is plotted. It can be observed that the vehicle consistently avoids collision with obstacles and successfully arrives at the desired goal position every time. In Fig. 13c, composite images captured during the experiment is presented.

2. Multiple Vehicles

One of the strengths of panel method based guidance algorithm is its ability to generate a collision free paths in real-time for multiple vehicles simultaneously. Unfortunately the platform shown in Fig. 5b consist of only a single quad-rotor. Consequently, an off-the-shelf platform namely Tello EDU Quad-Rotors (Fig. 14) are utilized to perform indoor experiments with multiple aerial vehicles.

In the experiments with multiple aerial vehicles, each vehicle has its own starting position and destination. Vehicle trajectories for two example scenarios are plotted in Figures 15 and 18. In Fig. 15a and Fig. 18a trajectories generated in



Fig. 14 Tello EDU Quad-rotor

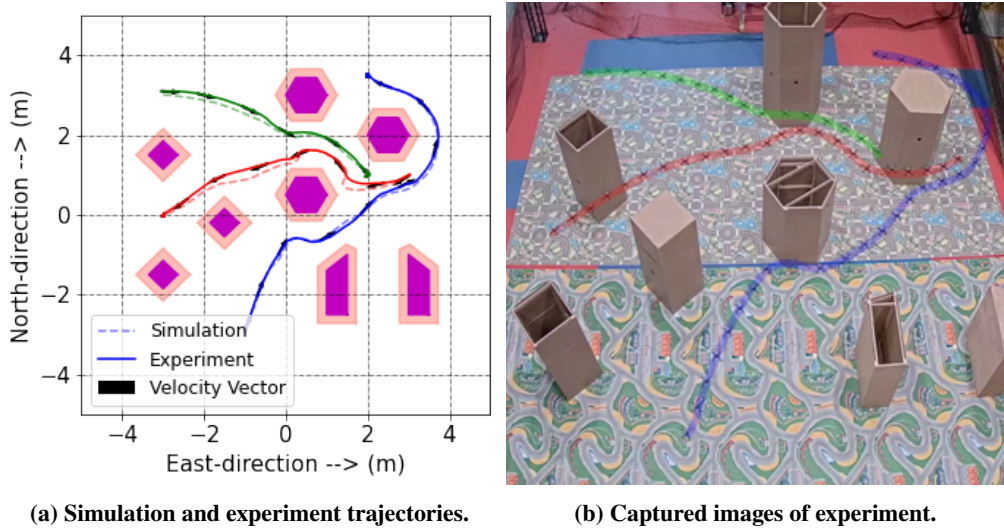


Fig. 15 Experiment 2. Three aerial vehicles travel to different destinations simultaneously while avoiding collision with buildings and each other.

simulation for three aerial vehicles are plotted together with actual paths followed by the vehicles during the experiment. Dashed lines are the trajectories generated in simulation and solid lines are the actual trajectories of the vehicles. Black arrows plotted on the trajectories are the velocity vectors commanded to the vehicles at given time steps. The difference between simulation paths and actual paths are mostly due to imprecise positioning of the vehicles at the start of experiments. In hardware experiments with multiple aerial vehicles, when one vehicle starts from a different position than the simulation not only it rides a different streamline, but also due to repulsive forces between the vehicles, the other vehicles generate different paths even if they have started at the exact same location as the simulation. Nonetheless, regardless of their starting positions, each vehicle can reach their destination without colliding with buildings or the other vehicles. Composite images generated with camera snapshots of hardware experiment for scenario 2 and scenario 3 are presented in Fig 15b and Fig. 18b respectively.

In Figure 16 sequential plots of resultant trajectories for the three vehicles for Experiment 2 are given. Sequential plots suggest that there are no collision between vehicles. Desired velocity input and measured velocity of Vehicle 1 (red on

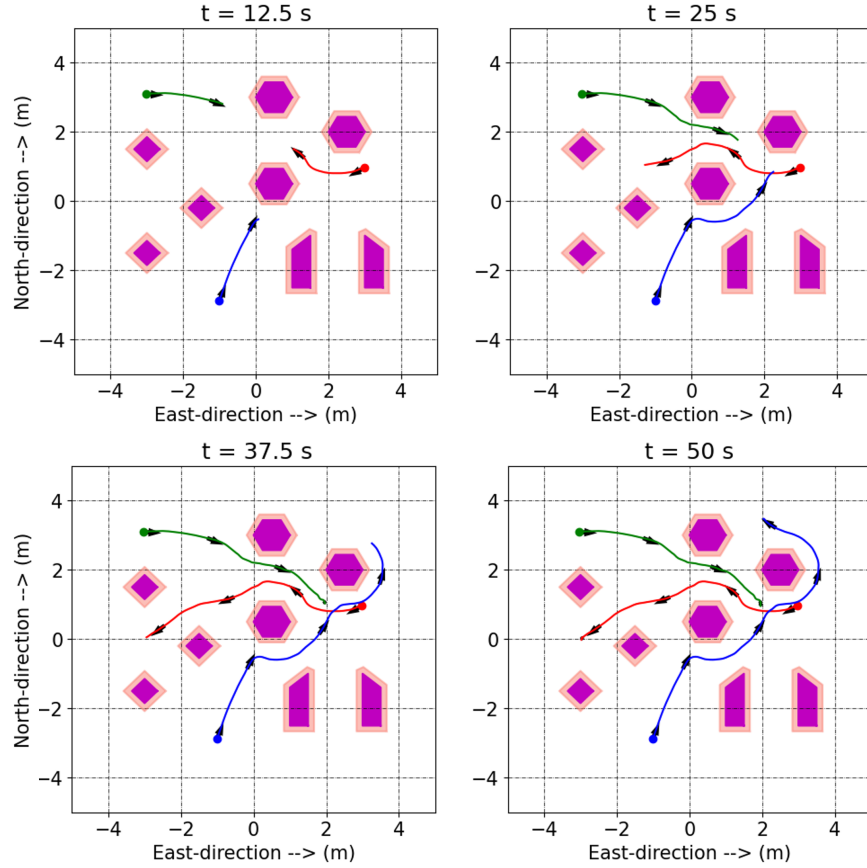


Fig. 16 Experiment 2, sequential figures.

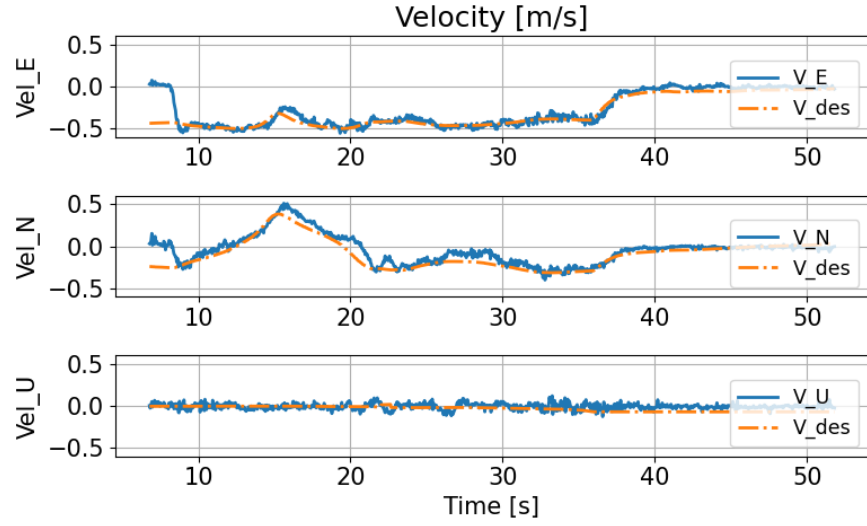
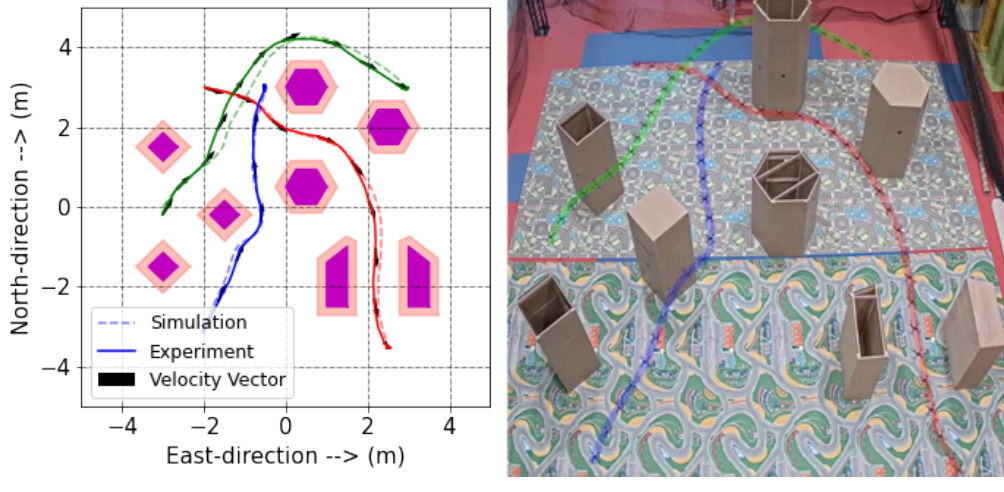


Fig. 17 Experiment 2, desired velocity and measured velocity of Vehicle 1 (Red).

Fig. 15) is plotted in Figure 17. Here, desired velocity is bounded to 0.5 m/s so that vehicle dynamics do not dominate the resultant paths.



(a) Simulation and experiment trajectories.

(b) Captured images of experiment.

Fig. 18 Experiment 3. Three aerial vehicles travel to different destinations simultaneously while avoiding collision.

C. Indoor Tests with WindShape

To test the robustness of the algorithm under effects of unknown wind gusts the wind generator shown in Fig. 8 is used. *WindShape* is a modular wind generator located inside ENAC's indoor flight facility.

1. Effect of Correction Term

To assess the effectiveness of panel method under wind disturbance three basic cases are considered and plotted on Fig. 19. First, to compare the performance of panel method and wind correction term, both methods are tested in an empty arena under wind disturbance. Results are presented in Fig. 19a. Here, wind speed (measured at the exit of WindShape) is gradually increased from 0m/s to 10m/s and the vehicle is tasked with flying on a straight line. In Fig. 19a, solid lines are the trajectories obtained from panel method solution and dashed lines are trajectories generated by panel method with correction term. The improvement introduced by the correction term is evident in this plot. Especially at higher wind speeds correction term reduces the deviation from original path significantly. Therefore, for the rest of the experiments panel method with correction term is used for path planning.

For the second case, a building is placed downstream of the wind to check whether the wind disturbance can cause a collision to an obstacle. As it can be observed from Fig. 19b, the vehicle avoids the building when the the wind speed is as high as 7m/s . However, this time the vehicle overshoots as soon as it exits the WindShape cone. This sort of overshoot is expected since there is a sudden change in wind speed at the exit of wind generator cone and velocity correction only uses instantaneous velocity error as opposed to prediction of desired path multiple steps ahead. Hence, for the third case, an other building is placed at the overshooting position to check whether this overshoot movement

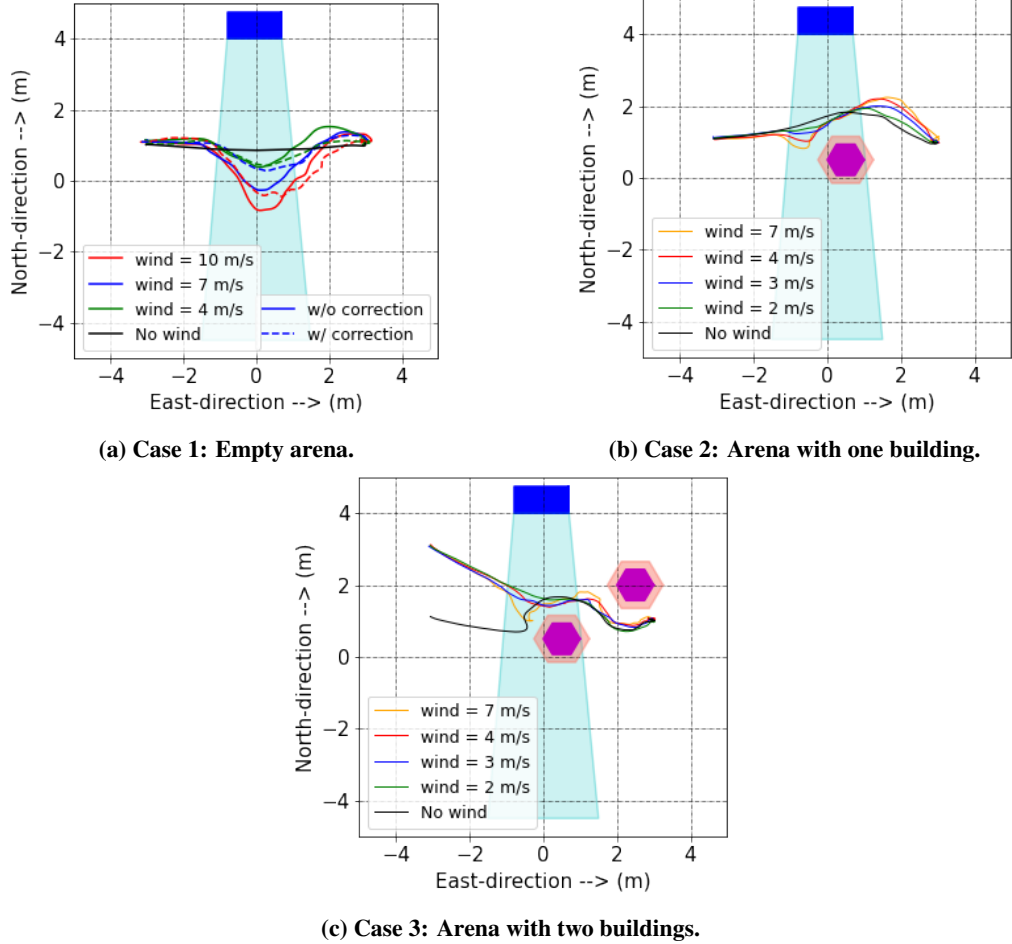


Fig. 19 Trajectories under wind disturbance for 3 cases. Even under effects of wind disturbance, collision avoidance is satisfied.

would cause a collision. In Fig. 19c, trajectories for the third case are plotted. In this scenario, in order to force the vehicle between buildings starting position is shifted 1m towards north. In this case too, panel method prevents collision with both obstacles under wind gust.

2. Single Vehicle

In Fig. 20, an example scenario for a single vehicle in a scaled urban environment is plotted. For this scenario the vehicle is tasked with traveling between its start position in north west and its destination in south east. This mission requires the vehicle to travel downstream in wind cone generated by WindShape. In Fig. 20a, trajectory logs from experiments conducted at different wind speeds are plotted together. Although the disturbance caused by the wind is evident, the vehicle arrives to its destination without much deviation from the original path. In Fig. 20b, sequential image captures from the experiment with wind speed of 4m/s are presented.

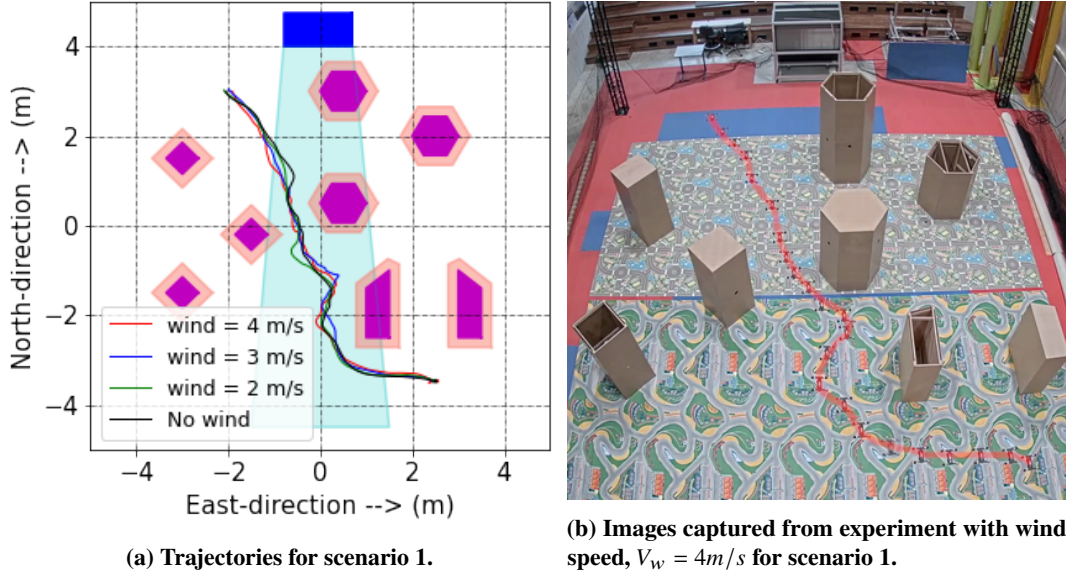


Fig. 20 Scenario 1: Single vehicle travelling downstream in wind cone.

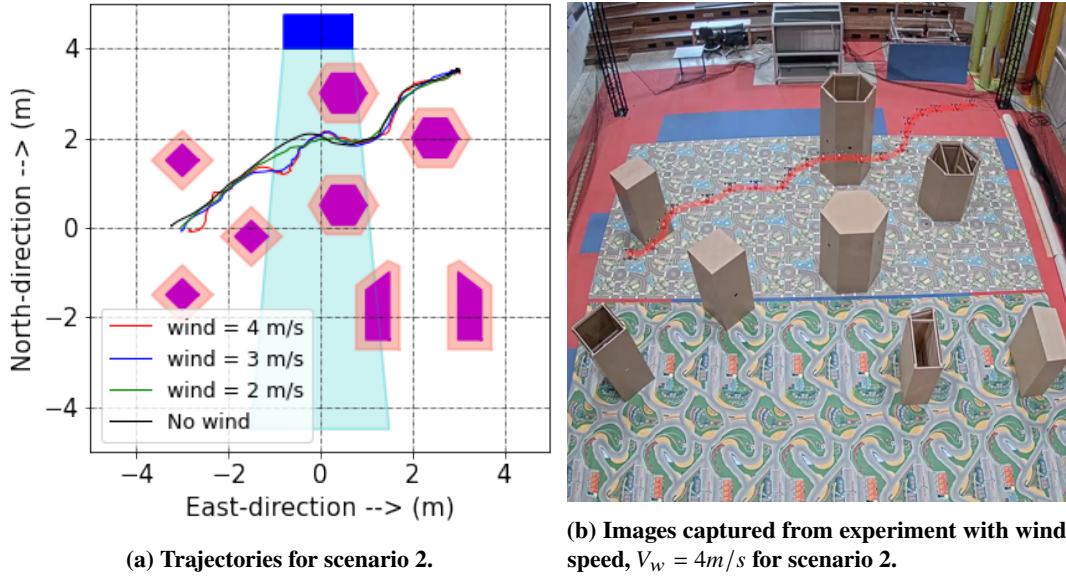


Fig. 21 Scenario 2: Travelling across wind cone.

Second example scenario where a vehicle is tasked with travelling from west to east is presented in Fig. 21. In this mission the vehicle has to travel across the wind cone generated by WindShape. In Fig. 21a, trajectory logs from experiments conducted at different wind speeds are plotted together. Especially at high wind speeds there is visible deviation from the original path. Nonetheless, the vehicle follows a collision free path and arrives to the desired destination. In Fig. 21b, sequential image captures from the experiment with wind speed of 4 m/s are presented.

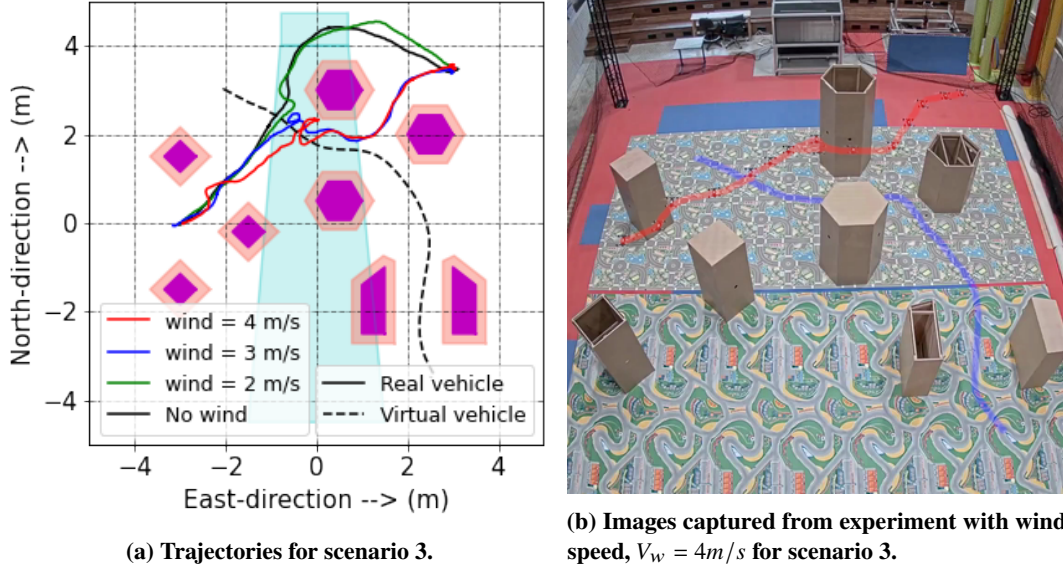


Fig. 22 Scenario 3: Guidance for a real vehicle and a virtual vehicle. The virtual vehicle has the same sensors and dynamics as the real vehicle.

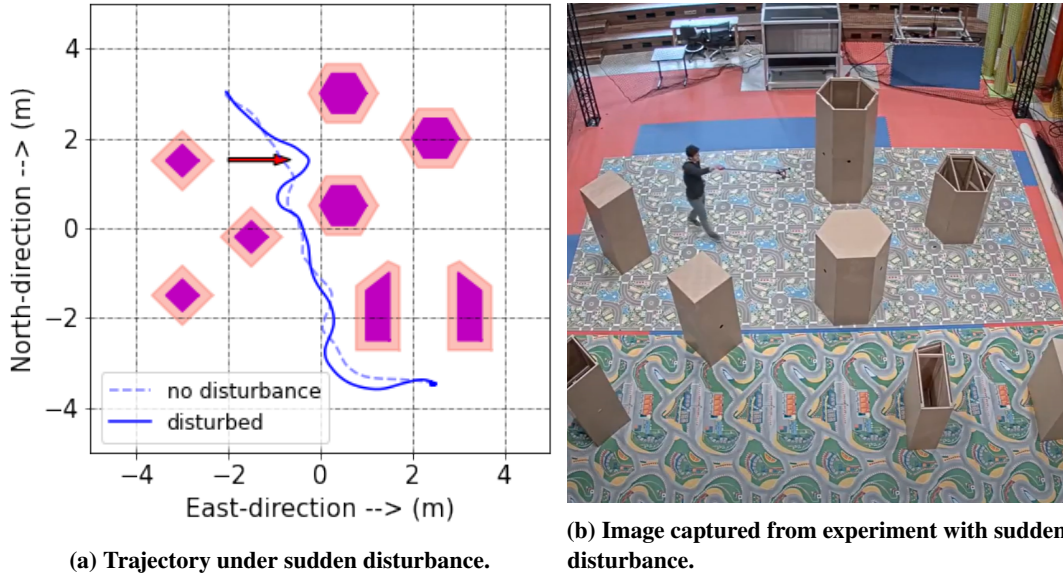


Fig. 23 Scenario 4: Sudden discrete disturbance. The vehicle is pushed with a stick at the position marked with the red arrow.

3. Multiple vehicles

For urban mobility applications, planning collision free paths for multiple aerial vehicles is a necessity. To that end, a virtual vehicle is included to the experiments throughout Paparazzi's dynamic simulation. The virtual vehicle has the same sensors and dynamics as the real vehicle; however, it does not experience the wind disturbance generated by WindShape. Experiment with the virtual vehicle is presented in Fig. 22. Here, the mission of the virtual vehicle is to travel from north east to its goal in south west. Similarly, the real vehicle travels from west to east. Both aerial

vehicles are modelled as point source elements in calculations to prevent any collisions. Furthermore, this experiment is conducted under different wind speeds. In Fig. 22a, trajectory logs from experiments conducted at different wind speeds are plotted together. To avoid collision with the virtual vehicle, real vehicle follows a path around hexagonal buildings. However, when the wind speed is larger than 3m/s , the real vehicle is forced to take the path between hexagonal buildings. In either case, there is no collision with the virtual vehicle. In Fig. 22b, sequential image captures from the experiment with wind speed of 4m/s are presented.

4. Discrete Disturbance

The last but not least, a final scenario for indoor arena is presented in Fig. 23. In this scenario a different type of disturbance is considered which is other than wind. The vehicle is tasked with travelling from north west to south east. At the position indicated with the red arrow in Fig. 23a the quad-rotor is pushed towards east with a stick. Although this sudden impact places the vehicle on a different streamline, using panel method a velocity vector that guarantees collision avoidance and convergence to goal position can be found at any empty position on the map. Hence, the vehicle can still avoid buildings and arrive at its destination. The disturbance neither causes any collision nor prevents the vehicle from reaching its goal.

D. Outdoor Tests

Outdoor experiments are conducted in a local RC airfield runway located in Muret, France, as shown in Fig. 7a. For the outdoor scenarios, there are no real buildings on the test area. Instead, no-fly zones with different shapes are

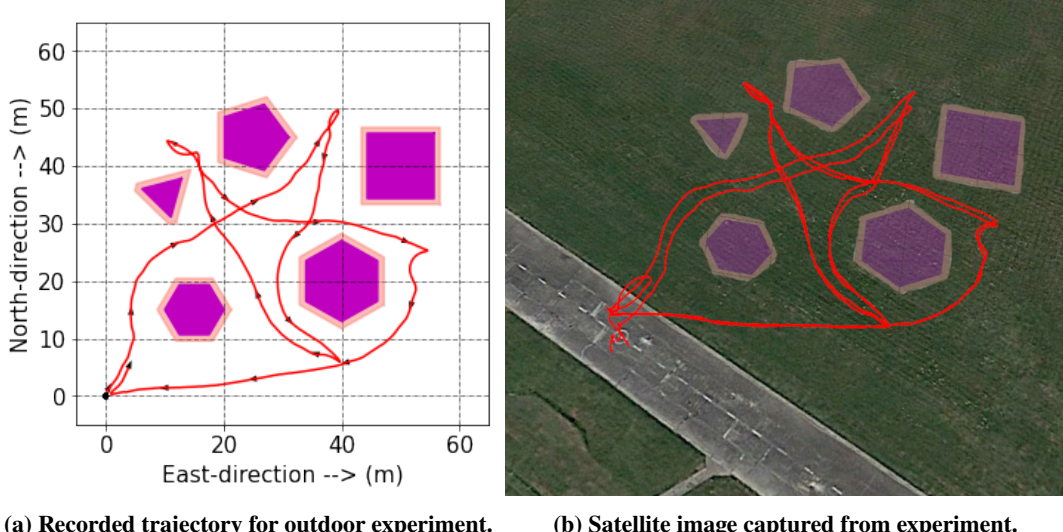


Fig. 24 Outdoor experiment with single vehicle. The vehicle is tasked with traveling between 5 goal positions consecutively.

defined on the outdoor arena. No-fly zones are marked with magenta colored polygons on the map as shown in Fig.

24b. Similar to indoor tests, no-fly zones are also inflated as a safety precaution. Inflated boundaries are plotted with shaded pink color. Safety perimeter for outdoor experiments were taken as 1m (as opposed to 20cm safety perimeter in indoor arena) due to greater sensor errors that had to be considered such as GPS accuracy, heading information from magnetometer, etc...

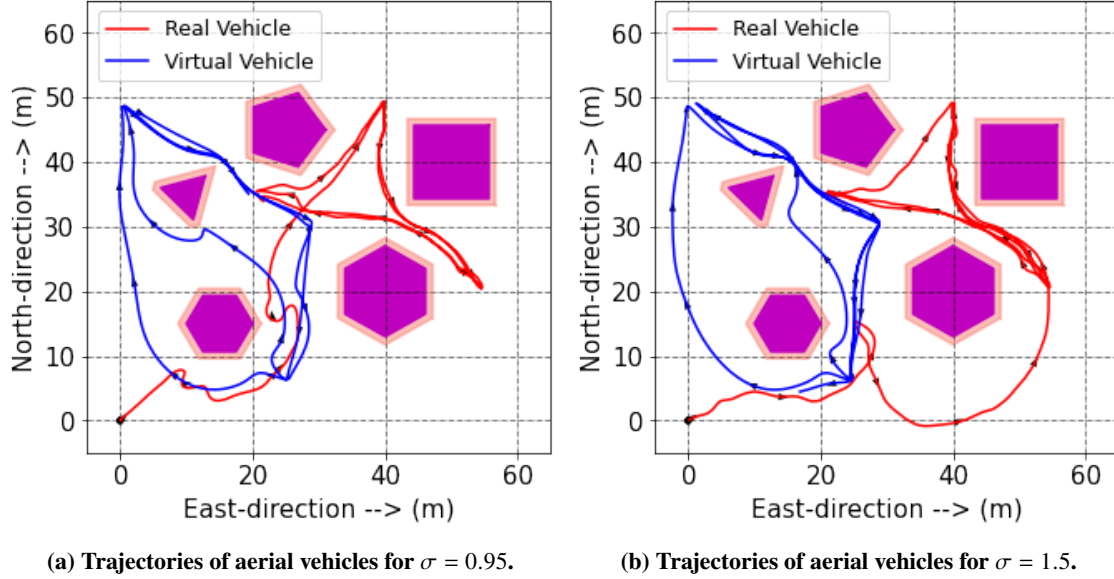


Fig. 25 Outdoor experiment with one real and one virtual vehicle.

1. Single Vehicle

In Fig. 24, outdoor experiment for a single vehicle is plotted. For this scenario, the vehicle starts from origin and is tasked with traveling to four goal positions sequentially and returning to origin again. Trajectory of the vehicle is plotted in Fig. 24a and satellite image capture from the experiment is presented in Fig. 24b.

2. Multiple vehicles

In Fig. 25, outdoor experiments with one real and one virtual vehicle are presented. The virtual vehicle has the same sensors and dynamics as the real vehicle. Both vehicles are tasked with travelling between 3 different goal positions sequentially while avoiding each other and no-fly zones. In Fig. 25a, trajectories of an experiment with relatively low source strength is given. In this case, both vehicles enter narrow corridors between no-fly zones and do not alter their path until they get close enough to the other vehicle. For the second case plotted in Fig. 25b, same scenario is repeated with larger source strength. This time, instead of entering narrow passages between no-fly zones, the vehicles take a detour around virtual obstacles and avoid each other completely.

VI. Conclusion

In this study, panel method based guidance algorithm for unmanned aerial vehicles for air mobility in urban environments is developed and robustness and effectiveness of the proposed algorithm is evaluated through hardware experiments in indoor and outdoor test facilities.

Panel method based guidance algorithm generates guidance vectors that can lead multiple aerial vehicles through collision free paths around obstacles with any size and shape. Since the vector field generated by panel method equations has no local minima, guidance vectors always lead the vehicle towards the goal position. Proposed algorithm has little computational load and is suitable for real-time applications.

This study introduces a new *safety source* element to steer the vehicles further away from obstacles as an additional safety precaution. The strength of the *safety source* element can be adjusted depending on the vehicle capabilities or safety requirements. Changing the magnitude of the source element does not bring any additional computational load; hence, this parameter can even be adjusted online.

A possible downside of panel method solution is that, for obstacle avoidance, positions and shapes of the buildings in a city have to be known beforehand. Still, it is not unrealistic to have this information with current mapping tools. Panel method is sensitive to size and number of panels, suitable number of panels are required to represent obstacles and have obstacle avoidance. Moreover, panel method based guidance algorithm does not guarantee generating time or distance optimal paths. However, the paths generated by the method are smooth and natural which makes it easier for aerial vehicles to follow.

In this study, obstacle avoidance and collision avoidance performance of panel method based guidance algorithm is tested using multiple quad-rotors in a scaled urban environment built in an indoor flight arena. Experimental results suggest that, proposed algorithm can successfully guide multiple aerial vehicles in cluttered environments without collision in real-time. Furthermore, obstacle avoidance and goal convergence capabilities of the panel method based guidance algorithm under wind gust disturbances are evaluated through indoor and outdoor test campaigns. Panel method based guidance algorithm is inherently robust against disturbances as it does not plan any paths but instead generates guidance vectors that lead to the goal position. In order to reduce the deviation under strong wind disturbances, a correction term is introduced and fed back to the velocity calculation with a PD controller. Experimental results suggest that proposed algorithm is robust against wind disturbances. Even under effect of wind, the vehicles can avoid obstacles and arrive desired goal positions.

Robustness of the proposed guidance algorithm is further tested with outdoor experiments where not only there were wind disturbances but also greater sensor errors had to be considered such as GPS accuracy, heading information from magnetometer, etc... Outdoor experiments are conducted with virtual no-fly zones instead of buildings as obstacles. In an open area with no buildings to disturb the wind flow, the effect of wind around buildings could not be observed.

To conclude, both indoor and outdoor flight tests suggests that panel method based guidance algorithm is a promising

tool for real-time guidance for air mobility in urban environments with decent disturbances rejection and guaranteed global convergence.

Acknowledgments

Authors would like to thank Cédric Boutet and Laurent Lacaze for the construction of scaled urban environment at ENAC and Xavier Paris for the indoor flight arena technical support and finally the open-source community of the Paparazzi Autopilot System. Through out this work Author Z. Bilgin was funded by Campus France.

References

- [1] Hansman, R., and Vascik, P., “Constraint Identification In On-Demand Mobility For Aviation Through An Exploratory Case Study Of Los Angeles,” 2018.
- [2] Bauranov, A., and Rakas, J., “Designing airspace for urban air mobility: A review of concepts and approaches,” *Progress in Aerospace Sciences*, Vol. 125, 2021, p. 100726. <https://doi.org/10.1016/j.paerosci.2021.100726>, URL <https://www.sciencedirect.com/science/article/pii/S0376042121000312>.
- [3] Ahamed, S., Prakash, S., Shuvrangshu, J., and Debasish, G., “UAS Flight Path Planning using Numerical Potential Fields in Dense Non-segregated Airspace,” *2021 International Conference on Unmanned Aircraft Systems (ICUAS)*, 2021, pp. 1010–1019. <https://doi.org/10.1109/ICUAS51884.2021.9476791>.
- [4] Zhang, N., Zhang, M., and Low, K. H., “3D path planning and real-time collision resolution of multirotor drone operations in complex urban low-altitude airspace,” *Transportation Research Part C: Emerging Technologies*, Vol. 129, 2021, p. 103123. <https://doi.org/10.1016/j.trc.2021.103123>, URL <https://www.sciencedirect.com/science/article/pii/S0968090X2100142X>.
- [5] Dai, W., Pang, B., and Low, K. H., “Conflict-free four-dimensional path planning for urban air mobility considering airspace occupancy,” *Aerospace Science and Technology*, Vol. 119, 2021, p. 107154. <https://doi.org/10.1016/j.ast.2021.107154>, URL <https://www.sciencedirect.com/science/article/pii/S1270963821006647>.
- [6] Huang, S., and Low, K. H., “A Path Planning Algorithm for Smooth Trajectories of Unmanned Aerial Vehicles via Potential Fields,” *2018 15th International Conference on Control, Automation, Robotics and Vision (ICARCV)*, 2018, pp. 1677–1684. <https://doi.org/10.1109/ICARCV.2018.8581198>.
- [7] Fiorini, P., and Shiller, Z., “Motion Planning in Dynamic Environments Using Velocity Obstacles,” *The International Journal of Robotics Research*, Vol. 17, No. 7, 1998, pp. 760–772. <https://doi.org/10.1177/027836499801700706>.
- [8] Petti, S., and Fraichard, T., “Safe Motion Planning in Dynamic Environments,” 2005, pp. 2210 – 2215. <https://doi.org/10.1109/IROS.2005.1545549>.

- [9] Fox, D., Burgard, W., and Thrun, S., “The Dynamic Window Approach to Collision Avoidance,” *Robotics and Automation Magazine, IEEE*, Vol. 4, 1997, pp. 23 – 33. <https://doi.org/10.1109/100.580977>.
- [10] Chan, N., Kuffner, J. J., and Zucker, M., “Improved Motion Planning Speed and Safety using Regions of Inevitable Collision,” 2008. URL <https://api.semanticscholar.org/CorpusID:16622850>.
- [11] Chakravarthy, A., and Ghose, D., “Obstacle Avoidance in a Dynamic Environment: A Collision Cone Approach,” *IEEE Transactions on Systems, Man, and Cybernetics—Part A: Systems and Humans*, Vol. 28, No. 5, 1998, pp. 570–574. <https://doi.org/10.1109/3468.709600>.
- [12] Chakravarthy, A., and Ghose, D., “Generalization of the Collision Cone Approach for Motion Safety in 3-D Environments,” *Autonomous Robots*, Vol. 32, No. 3, 2012, pp. 243–266. <https://doi.org/10.1007/s10514-011-9270-z>.
- [13] Chakravarthy, A., and Ghose, D., “Collision Cones for Quadric Surfaces,” *IEEE Transactions on Robotics*, Vol. 27, No. 6, 2011, p. 1166. <https://doi.org/10.1109/TRO.2011.2159413>.
- [14] Mirzaei Teshnizi, M., Kosari, A., Goliae, S., and Shakeshi, S., “Centralized Path Planning for Multi-aircraft in the Presence of Static and Moving Obstacles,” *International Journal of Engineering*, Vol. 33, No. 5, 2020, pp. 923–933. <https://doi.org/10.5829/ije.2020.33.05b.25>.
- [15] Chen, Y., Luo, G., Mei, Y., Yu, J., and Su, X., “UAV path planning using artificial potential field method updated by optimal control theory,” *International Journal of Systems Science*, Vol. 47, 2016, pp. 1407 – 1420. URL <https://api.semanticscholar.org/CorpusID:29757767>.
- [16] Ge, D., and Topcu, U., “Hierarchical Path Planning for Urban On-Demand Air Mobility,” *2019 IEEE Conference on Control Technology and Applications (CCTA)*, 2019, pp. 894–899. <https://doi.org/10.1109/CCTA.2019.8920446>.
- [17] Pradeep, P., and Wei, P., “Energy-Efficient Arrival with RTA Constraint for Multirotor eVTOL in Urban Air Mobility,” *Journal of Aerospace Information Systems*, Vol. 16, 2019. <https://doi.org/10.2514/1.I010710>.
- [18] Khatib, O., “Real-time obstacle avoidance for manipulators and mobile robots,” *Proceedings. 1985 IEEE International Conference on Robotics and Automation*, Vol. 2, 1985, pp. 500–505. <https://doi.org/10.1109/ROBOT.1985.1087247>.
- [19] Orozco-Rosas, U., Montiel, O., and Sepúlveda, R., “Mobile robot path planning using membrane evolutionary artificial potential field,” *Applied Soft Computing Journal*, 2019, pp. 236–251. <https://doi.org/10.1016/j.asoc.2019.01.036>.
- [20] Lifen, L., Ruoxin, S., Shuandao, L., and Jiang, W., “Path planning for UAVS based on improved artificial potential field method through changing the repulsive potential function,” *2016 IEEE Chinese Guidance, Navigation and Control Conference (CGNCC)*, 2016, pp. 2011–2015. <https://doi.org/10.1109/CGNCC.2016.7829099>.
- [21] Yingkun, Z., “Flight path planning of agriculture UAV based on improved artificial potential field method,” *2018 Chinese Control And Decision Conference (CCDC)*, 2018, pp. 1526–1530. <https://doi.org/10.1109/CCDC.2018.8407369>.

- [22] Liu, Y., and Zhao, Y., “A virtual-waypoint based artificial potential field method for UAV path planning,” *2016 IEEE Chinese Guidance, Navigation and Control Conference (CGNCC)*, 2016, pp. 949–953. <https://doi.org/10.1109/CGNCC.2016.7828913>.
- [23] Honglun, W., Wentao, L., Yao, P., Liang, X., and Chang, L., “Three-dimensional Path Planning for Unmanned Aerial Vehicle Based on Interfered Fluid Dynamical System,” *Chinese Journal of Aeronautics*, Vol. 28, 2014. <https://doi.org/10.1016/j.cja.2014.12.031>.
- [24] Bayat, F., Najafi-Nia, S., and Aliyari, M., “Mobile Robots Path Planning: Electrostatic Potential Field Approach,” *Expert Systems with Applications*, Vol. 100, 2018. <https://doi.org/10.1016/j.eswa.2018.01.050>.
- [25] Nazarahari, M., Khanmirza, E., and Doostie, S., “Multi-objective multi-robot path planning in continuous environment using an enhanced Genetic Algorithm,” *Expert Systems with Applications*, Vol. 115, 2018. <https://doi.org/10.1016/j.eswa.2018.08.008>.
- [26] Tsourveloudis, N., Valavanis, K., and Hebert, T., “Autonomous Vehicle Navigation Utilizing Electrostatic Potential Fields and Fuzzy Logic,” *Robotics and Automation, IEEE Transactions on*, Vol. 17, 2001, pp. 490 – 497. <https://doi.org/10.1109/70.954761>.
- [27] Li, H., Liu, W., Yang, C., Wang, W., Qie, T., and Xiang, C., “An Optimization-based Path Planning Approach for Autonomous Vehicles using dynEFWA-Artificial Potential Field,” *IEEE Transactions on Intelligent Vehicles*, 2021, pp. 1–1. <https://doi.org/10.1109/TIV.2021.3123341>.
- [28] Li, W., Yang, C., Jiang, Y., Liu, X., and Su, C.Y., “Motion Planning for Omnidirectional Wheeled Mobile Robot by Potential Field Method,” *Journal of Advanced Transportation*, Vol. 2017, 2017, pp. 1–11. <https://doi.org/10.1155/2017/4961383>.
- [29] Hosseini Rostami, S. M., Kumar, A., Wang, J., and Liu, X., “Obstacle avoidance of mobile robots using modified artificial potential field algorithm,” *EURASIP Journal on Wireless Communications and Networking*, Vol. 2019, 2019. <https://doi.org/10.1186/s13638-019-1396-2>.
- [30] Chester, C. R., “Techniques in Partial Differential Equations,” *McGraw-Hill*, 1970, pp. 72–73.
- [31] Kim, J.-O., and Khosla, P., “Real-time obstacle avoidance using harmonic potential functions,” *IEEE Transactions on Robotics and Automation*, Vol. 8, No. 3, 1992, pp. 338–349. <https://doi.org/10.1109/70.143352>.
- [32] Masoud, A. A., “A harmonic potential field approach for joint planning and control of a rigid, separable nonholonomic, mobile robot,” *Robotics and Autonomous Systems*, Vol. 61, No. 6, 2013, pp. 593–615. <https://doi.org/10.1016/j.robot.2013.02.007>, URL <https://www.sciencedirect.com/science/article/pii/S0921889013000432>.
- [33] Fahimi, F., “Autonomous robots,” *Springer*, 2010, pp. 81–127.
- [34] Daily, R., and Bevly, D. M., “Harmonic potential field path planning for high speed vehicles,” *2008 American Control Conference*, 2008, pp. 4609–4614. <https://doi.org/10.1109/ACC.2008.4587222>.
- [35] Garrido, S., and Moreno, L., “Robotic Navigation using Harmonic Functions and Finite Elements.” 2006, pp. 94–103.

- [36] Liang, X., Honglun, W., Li, D., and Liu, C., “Three-dimensional path planning for unmanned aerial vehicles based on fluid flow,” 2014, pp. 1–13. <https://doi.org/10.1109/AERO.2014.6836520>.
- [37] Pimenta, L. C. A., Pereira, G. A. S., Michael, N., Mesquita, R. C., Bosque, M. M., Chaimowicz, L., and Kumar, V., “Swarm Coordination Based on Smoothed Particle Hydrodynamics Technique,” *IEEE Transactions on Robotics*, Vol. 29, No. 2, 2013, p. 383. <https://doi.org/10.1109/TRO.2013.2243998>.
- [38] Song, Z., Lipinski, D., and Mohseni, K., “Multi-vehicle cooperation and nearly fuel-optimal flock guidance in strong background flows,” *Ocean Engineering*, Vol. 141, 2017, pp. 388–404. <https://doi.org/10.1016/j.oceaneng.2017.05.024>.
- [39] Lewis, R. I., *The surface vorticity method for inviscid ideal fluid flow*, Cambridge Engine Technology Series, Cambridge University Press, 1991, pp. 3–98.
- [40] Katz, J., and Plotkin, A., *Singularity Elements and Influence Coefficients*, 2nd ed., Cambridge Aerospace Series, Cambridge University Press, 2001, p. 230–261. <https://doi.org/10.1017/CBO9780511810329.012>.
- [41] Anderson, J. D., “Fundamentals of Aerodynamics,” *McGraw-Hill*, 2011, pp. 319–325.
- [42] Zhang, Y., and Valavanis, K. P., “A 3-D Potential panel method for robot motion planning,” *Robotica*, Vol. 15, 1997, pp. 421 – 434. <https://doi.org/10.1017/S0263574797000520>.
- [43] Velagić, J., Vuković, L., and Ibrahimović, B., “Mobile Robot Motion Framework Based on Enhanced Robust Panel Method,” *International Journal of Control, Automation and Systems*, Vol. 18, No. 5, 2020, pp. 1264–1276. <https://doi.org/https://doi.org/10.1007/s12555-019-0009-5>.
- [44] Uzol, O., Yavrucuk, I., and Sezer Uzol, N., “Panel-Method-Based Path Planning and Collaborative Target Tracking for Swarming Micro Air Vehicles,” *Journal of Aircraft - J AIRCRAFT*, Vol. 47, 2010, pp. 544–550. <https://doi.org/10.2514/1.45469>.
- [45] ENAC, “Drone Flight Arena Toulouse Occitanie,” Ecole Nationale de l’Aviation Civile, Retrieved 19 October 2021, from <https://www.enac.fr/en/drone-flight-arena-toulouse-occitanie-0>, 2021.
- [46] Maxwell, J. C., “On Physical Lines of Force,” *Philosophical Magazine Series 4*, Vol. 21, No. 139, 1861, pp. 161–175. <https://doi.org/10.1080/14786446108643680>.
- [47] Bilgin, Z., Bronz, M., and Yavrucuk, I., “Experimental Evaluation of Panel-Method-Based Path Planning for eVTOL in A Scaled Urban Environment,” *Vertical Flight Society Forum* 78, 2022. <https://doi.org/10.4050/F-0078-2022-17536>.
- [48] Smeur, E., de Croon, G., and Chu, Q., “Cascaded incremental nonlinear dynamic inversion for MAV disturbance rejection,” *Control Engineering Practice*, Vol. 73, 2018, pp. 79–90. <https://doi.org/https://doi.org/10.1016/j.conengprac.2018.01.003>, URL <https://www.sciencedirect.com/science/article/pii/S0967066118300030>.
- [49] Panerati, J., Zheng, H., Zhou, S., Xu, J., Prorok, A., and Schoellig, A., “Learning to Fly—a Gym Environment with PyBullet Physics for Reinforcement Learning of Multi-agent Quadcopter Control,” , 03 2021.

[50] Hattenberger, G., Bronz, M., and Gorraz, M., “Using the Paparazzi UAV System for Scientific Research,” 2014. <https://doi.org/10.4233/uuid:b38fbdb7-e6bd-440d-93be-f7dd1457be60>.